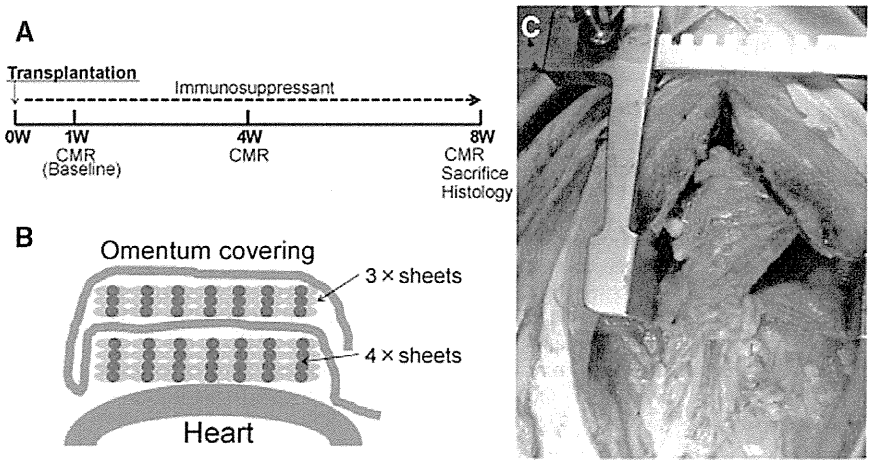

Figure 1. Study protocol of the mini-pig experiment and operative procedure. **A**, Schedule of cardiac MRI (CMR) and histological evaluations. **B**, Procedural scheme of cell-sheet transplantation with the omentum. **C**, Image taken after treatment. The omentum is mobilized and transplanted with the cell sheets on the heart through median sternotomy with an additional upper midline laparotomy.

cells in each field was counted using a light microscope under high-power magnification (×200). The stained blood vessels from the 10 fields were averaged and the results expressed as vascular density (per square millimeter). The frozen sections were immunolabeled with anti-cTNT antibody (1:100 dilution; Abcam, Cambridge, UK) and anti-CD68 antibody for macrophages (1:100 dilution, Abcam) as primary antibodies and visualized with AlexaFluor488–conjugated goat anti-mouse (Invitrogen) and AlexaFluor555–conjugated goat anti-rabbit (Invitrogen) as secondary antibodies. Nuclei were counterstained with 4′,6-diamidino-2-phenylindole (Dojindo, Tokyo, Japan) and assessed using the Biorevo BZ-9000 (Keyence) or confocal microscopy (Olympus Japan, FV1000-D IX81, Tokyo, Japan). SPIO particles of Prussian blue staining were visualized by differential interference contrast of confocal microscopy.

Real-Time Polymerase Chain Reaction

Total RNA was extracted from cardiac tissue and reverse transcribed using Omniscript reverse transcriptase (Qiagen, Hilden, Germany) with random primers (Invitrogen), and the resulting cDNA was used for real-time polymerase chain reaction with the ABI PRISM 7700 (Applied Biosystems, Stockholm, Sweden) system using pig-specific primers (Applied Biosystems) for vascular endothelial growth factor (VEGF), basic fibroblast growth factor, and stromal-derived factor-1 (SDF-1). Each sample was analyzed in triplicate for each gene studied. Data were normalized to GAPDH expression level. For relative expression analysis, the delta-delta Ct method was used, and values of the cell-sheet transplantation without the omentum were used as reference values.

Statistical Analysis

Data are expressed as means±SDs. Comparisons between 2 groups were made using Welch t test. Cell survival proportion over time was assessed by repeated-measures ANOVA with group, time, and group×time interaction effects. All P values are 2-sided, and values of $P<0.05$ were considered to indicate statistical significance. Statistical analyses were performed using JMP 9.02 (SAS Institute, Cary, NC).

Results

Generation of SPIO-Labeled hiPS-CM Cell Sheets

Cardiomyogenic differentiation of hiPS cells was induced by treatment of the embryoid bodies formed from cultured hiPS cells with Wnt3a and R-spondin-1. Subsequently, the differentiated hiPS cells were purified by culture in glucose-free medium to yield ≈1 to 2×10^7 hiPS-CMs. Approximately 80% (83.6±8.1%) of the hiPS-CMs were positive for cTNT, as determined by flow cytometry (Figure 2A). After SPIO labeling to the hiPS-CMs, human mesenchymal stem cells were added to the hiPS-CM culture. Subsequently, culture in the thermoresponsive dishes yielded round-shaped hiPS-CM cell sheets (Figure 2B). The hiPS-CMs on the sheet continued to beat before and after detaching from culture surface (Movies I and II in the online-only Data Supplement). Immunohistolabeling showed that the large number of cells in the hiPS-CM cell sheets were homogeneously positive for cTNT (Figure 2C). Prussian blue staining confirmed that the hiPS-CMs contained iron in the cytoplasm (Figure 2D).

In Vivo Analysis of Survival of Transplanted SPIO-Labeled hiPS-CMs by Serial CMR

Transplantation of the same number of hiPS-CM cell sheets with or without the omentum covering was successfully performed via median sternotomy in 16 normal mini-pigs. There was no mortality related to the procedure or otherwise before the planned euthanasia. In addition, the omentum was attached to the surface of the heart in all mini-pigs with the omentum. CMRs were performed to assess the survival of transplanted SPIO-labeled hiPS-CMs at 1 week (baseline), 4 weeks, and 8 weeks after cell transplantation.

SPIO signals were clearly identified as the hypointense area in the surface of the left ventricle by CMR in all mini-pigs throughout the study period (Figure 3A). SPIO-positive hypointense area was gradually decreased in both the groups during the 8 weeks, whereas the SPIO-positive area was larger and thicker in mini-pigs with the omentum compared with those without the omentum during the study period. The survival proportion of the SPIO-labeled hiPS-CMs was determined by the formula that the hypointense area at 4 and 8 weeks after transplantation was divided by the area at 1 week after transplantation as baseline. Both groups showed steady decrease in the cell survival during the 7 weeks, whereas the proportion of decrease was significantly less in mini-pigs with the omentum than in those without it at 4 weeks (92±10% versus 60±10%) and 8 weeks (78±10% versus 42±9%) after treatment ($P<0.0001$ for interaction effect of time and group in the repeated ANOVA; Figure 3B).

Histological Evaluation of Transplanted hiPS-CMs With or Without the Omentum

Excised heart tissues at 8 weeks after transplantation were assessed by histology. The transplanted hiPS-CMs and the

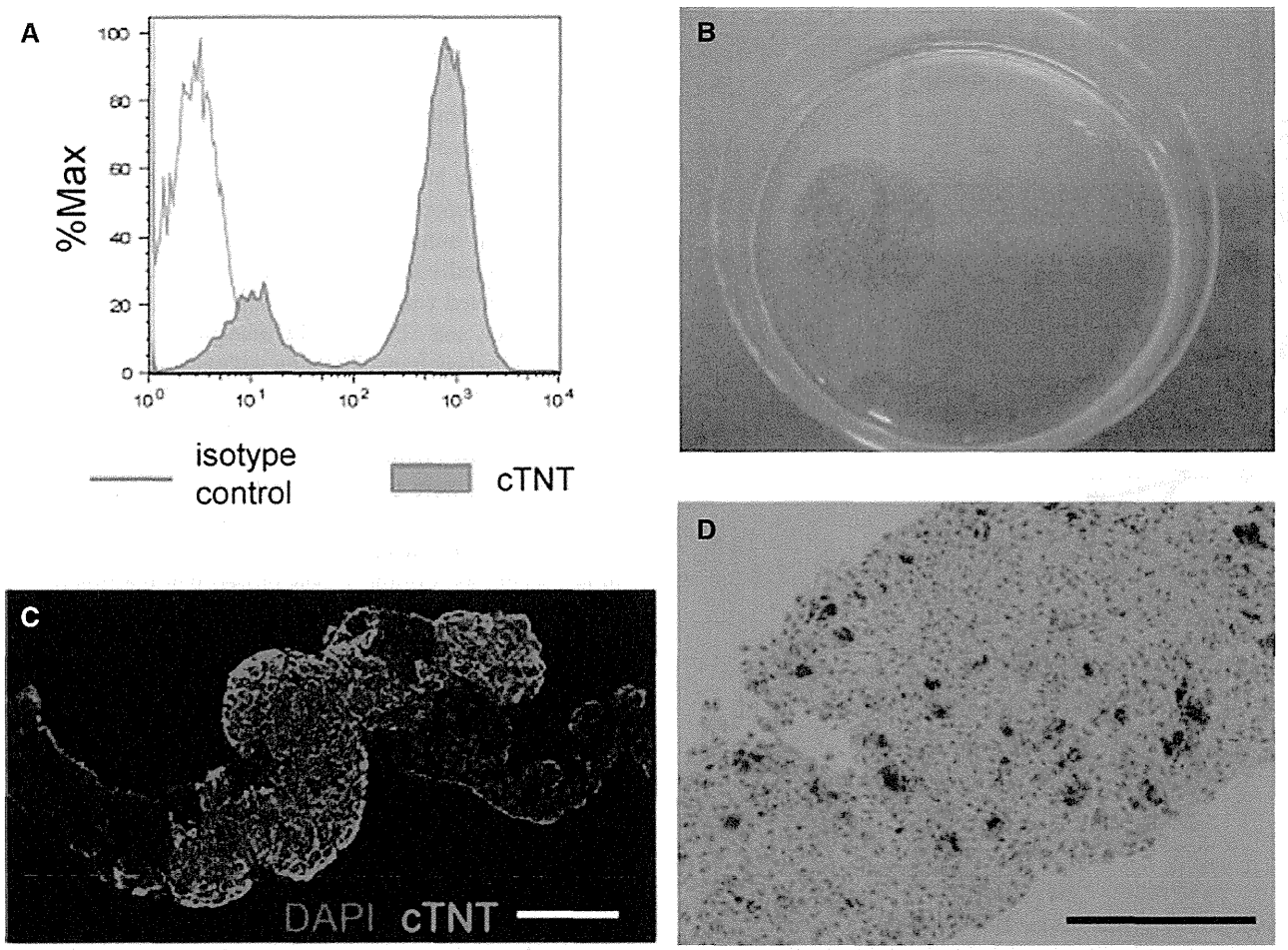

Figure 2. Histological characteristics of the human induced pluripotent stem cell–derived cardiomyocyte (hiPS-CM) cell sheet. **A**, Expression of cardiac troponin T (cTNT) after differentiation and purification of hiPS-CMs. **B**, A superparamagnetic iron oxide (SPIO)–labeled hiPS-CM cell sheet in a 10-cm dish. **C**, Immunostaining of the hiPS-CM cell sheet with cTNT antibody (green). The cell nuclei were counterstained with 4′,6-diamidino-2-phenylindole (DAPI; blue). **D**, Prussian blue staining of the SPIO-labeled hiPS-CM cell sheet. Scale bar, 50 μm in **C** and **D**.

pedicle omentum were attached over the epicardium of the left ventricle without any histological gaps in all mini-pigs, as assessed by hematoxylin–eosin staining (Figure 4D). The hearts without the omentum showed cellular and fibrous components over the anterior wall of the ventricles (Figure 4A), whereas the hearts with the omentum showed thick cellular, fibrous, and fat-rich components covering the anterior and lateral wall of the ventricles (Figure 4D).

Prussian blue staining revealed cells containing iron on the surface of the ventricles, corresponding to the area seen on CMR in both groups (Figure 4B and 4E). A larger number of cells with iron contents were identified in mini-pigs with the omentum compared with those without (Figure 4B, 4C, 4E, and 4F). In fact, the density of iron-containing cells in the transplanted site, assessed semiquantitatively by Prussian blue staining at 8 weeks after treatment, was significantly greater in the mini-pig with the omentum (27±6 cells/high-power field) than in those without it (5±2 cells/high-power field; $P<0.0001$; Figure 4G). Immunohistolabeling showed that a larger number of cells are positive for cTNT in the area where cells with iron inclusions are present in mini-pigs with the omentum compared with those without it (Figure 4H). The distribution of the SPIO particles was visualized by differential interference contrast of confocal microscopy. Grafted hiPS-CMs were identified and confirmed as double-positive for cTNT and SPIO and negative for CD68, which is a specific marker for macrophages, by immunohistolabeling (Figure 4I–4N). In addition, no teratomas were formed in the heart or other thoracic organs at 8 weeks after the transplantation of the hiPS-CM cell sheets with or without the omentum (data not shown).

Capillary Density in the Transplanted Area

Vessels and capillaries in the transplanted cell sheets at 8 weeks after transplantation were visualized and assessed by immunohistochemistry for von Willebrand factor. The transplanted cell sheets without the omentum contained a large number of capillaries and a small number of vessels in a homogeneous manner (Figure 5A), suggesting that vascular network was created possibly to support the survival and function of the cell sheets. Of note, the number of capillaries and vessels were markedly greater in the cell sheets covered by the omentum compared with those without it (Figure 5B). In fact, capillary density in the transplanted cell sheets, assessed semiquantitatively by immunohistochemistry for von Willebrand factor at 8 weeks after treatment, was significantly and markedly

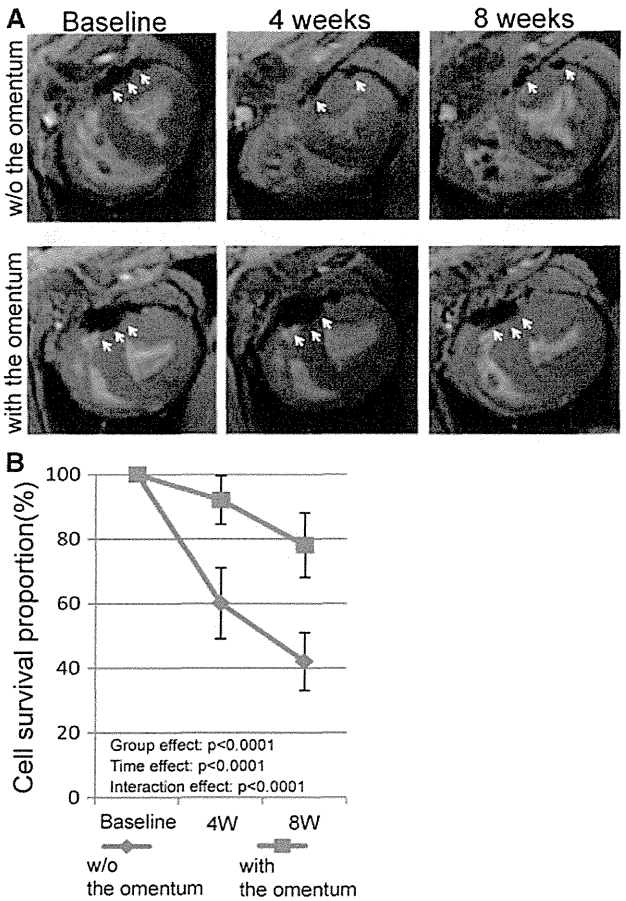

Figure 3. In vivo analysis of the survival of superparamagnetic iron oxide (SPIO)–labeled human induced pluripotent stem cell–derived cardiomyocytes (hiPS-CMs) after transplantation. **A**, Serial cardiac MRIs were examined at 1 week (baseline), 4 weeks, and 8 weeks after SPIO-labeled hiPS-CM cell-sheet transplantation, with or without the omentum. Representative hypointense area of the SPIO-labeled hiPS-CMs is indicated by white arrows. **B**, Cell survival proportion was estimated by the SPIO-labeled area at 4 and 8 weeks, corrected by cell survival at 1 week.

greater in mini-pigs with the omentum (64±21 U/mm^2) than in those without it (9±5 U/mm^2; P<0.0001; Figure 5C).

Upregulation of VEGF, Basic Fibroblast Growth Factor, and SDF-1 Expression in the Transplanted Area

The expression level of cardioprotective and angiogenic factors in the transplanted area at 8 weeks after treatment was quantitatively assessed by real-time polymerase chain reaction for VEGF, basic fibroblast growth factor, and SDF-1. The relative expression of all the factors in the transplanted area was significantly greater in mini-pigs with the omentum than in those without it (VEGF, 1.94±0.38 versus 1.35±0.26; P<0.05; basic fibroblast growth factor, 2.33±0.92 versus 1.21±0.19; P<0.05; SDF-1, 2.05±0.33 versus 1.22±0.21; P<0.01; Figure 6A–6C).

Discussion

It is herein demonstrated that our differentiation protocol yielded hiPS-CMs with >80% purity, and hiPS-CM cell sheets were transplanted over the anterior wall of the ventricle, covered by the pedicle omentum, in a porcine model without procedural failure or procedure-related morbidity/mortality. The number of surviving cTNT-positive hiPS-CMs on the native myocardium was significantly greater in mini-pigs with the omentum than in those without it, although there was a steady decrease in the surviving cell number, regardless of the omentum support, as assessed by SPIO cell labeling with CMR and by immunohistolabeling. The pedicle omentum covering markedly increases the number of vessels and capillaries, associated with the upregulation of VEGF, hepatocyte growth factor, and SDF-1, at the transplanted area compared with the cell-sheet transplantation without the omentum.

In the present study, SPIO-labeled hiPS-CMs were clearly visualized in vivo by CMR, corresponding to the histological findings that confirmed iron contents in the transplanted hiPS-CMs that were positive for cTNT, as reported by previous publications.[22,23] Using this method, the distribution and survival of the transplanted hiPS-CMs were serially evaluated in this study. As a result, it was proved that the unique technique in which transplanted cell sheets were covered by the pedicle omentum elicited a greater survival of the transplanted hiPS-CMs over the ventricular epicardial surface at 4 weeks compared with cell-sheet transplantation without the omentum covering. This suggests that pedicle omentum covering the cell sheets promptly induced angiogenesis to improve the hypoxic environment at the transplanted area, compared with the omentum-free method. In addition, although the size of the graft was decreased in both groups during the 8 weeks, trend in the size reduction was significantly milder in the omentum group than in the omentum-free group. This was consistent to the increased vascular network and upregulated angiogenic factors at the transplanted area in the omentum group at 8 weeks after the cell-sheet transplantation. These findings indicate that covering the cell sheet with the pedicle omentum that carries abundant angiogenic potentials[17–19] enhanced neovascular formation at the transplanted area promptly after transplantation and that vascular-rich structure at the transplanted area persisted long-term. In previous studies, antiapoptotic treatments on the transplanted cells, including upregulation of AKT[24] or overexpression of Bcl-2,[25] have been shown to improve survival after cell transplantation. We achieved to improve cell survival after transplantation by modifying the cell delivery method. The pedicled omental flap is frequently and safely applied for the treatment of mediastinitis after cardiovascular surgery. As cell transplantation is indicated to the patients with severe heart failure, we need to establish a minimally invasive approach to mobilize the omentum. Besides, we expect our unique combination method to be a feasible and safe treatment option in clinical settings. However, in this study, transplanted hiPS-CMs produced by our protocol may be immature, although they were spontaneously contractile. In the specimen 8 weeks after transplantation with the omentum, there were few surviving hiPS-CMs with organized sarcomeres in the cytoplasm, whereas there were many cTNT-positive cells (data not shown). In recent studies, mechanical load of hiPS-CMs in vitro controlled their alignment, proliferation, and hypertrophy,[26] and spontaneous and synchronous beating cardiac cell sheets were created by a bioreactor culture, which expanded and induced cardiac differentiation of hiPS cells.[27] It is necessary to modify

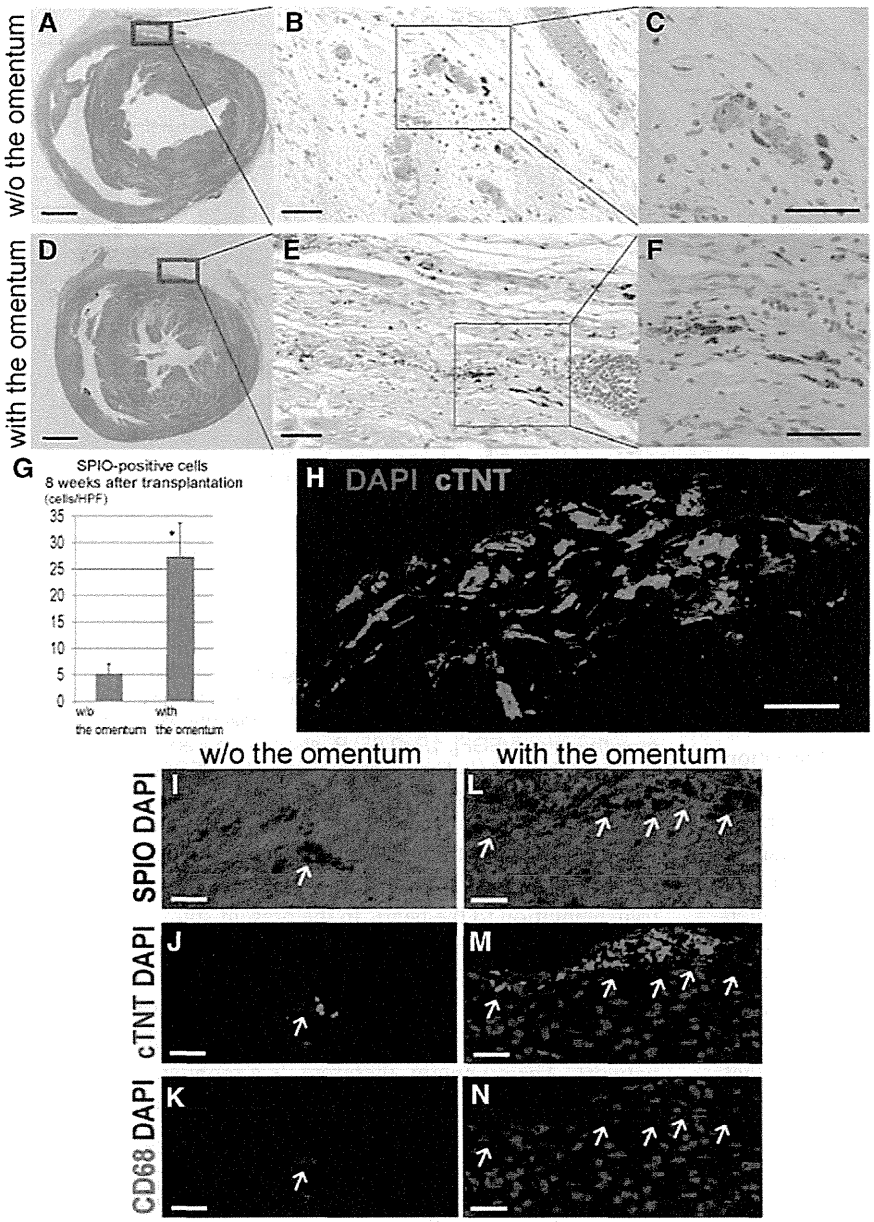

Figure 4. Human induced pluripotent stem cell–derived cardiomyocytes (hiPS-CMs) after transplantation. Macroscopic images of the whole heart by hematoxylin–eosin staining at the mid level in the mini-pig without (**A**) or with (**D**) the omentum; scale bar, 1 cm in **A** and **D**. Cells containing iron, indicative of superparamagnetic iron oxide (SPIO)–labeled hiPS-CMs, were detected by Prussian blue staining of sections of mini-pigs without (**B** and **C**) or with (**E** and **F**) the omentum at the transplanted area; scale bar, 50 μm in **B**, **C**, **E**, and **F**. **G**, The density of SPIO-positive cells in the transplanted site was semiquantitatively assessed at 8 weeks after treatment. **P*<0.0001 vs without the omentum. **H**, In the transplanted regions of mini-pigs with the omentum, cardiac troponin T (cTNT)–positive cells were also demonstrated by immunohistolabeling (green). The cell nuclei were counterstained with 4′,6-diamidino-2-phenylindole (DAPI; blue); scale bar, 50 μm in **H**. **I–N**, In the transplanted regions of mini-pigs, SPIO particles were visualized by differential interference contrast (DIC), and grafted hiPS-CMs, which were double-positive for cTNT (green) and SPIO (DIC) and negative for CD68 (red), were indentified by immunohistolabeling. The cell nuclei were counterstained with DAPI (blue). Arrows indicate SPIO particles, referred to DIC images in **I** and **L**; scale bar, 20 μm in **I–N**.

our hiPS-CM preparation protocols referred to in these studies to yield the amount of contracting hiPS-CMs contributing to the mechanical function of the injured heart. In addition, we previously demonstrated that maturation of iPS-CMs progressed after iPS-CMs were transplanted in nude rat heart.[28] Therefore, we also expect that improving environments after cell transplantation, such as avoiding delivered cell ischemia, inflammation, and immunogenic rejection, will promote in vivo differentiation of iPS-CMs and their therapeutic effects. The combination of hiPS-CM sheets and the omentum is a promising delivery method to differentiate hiPS-CMs in vivo, because the omentum at least prevents cell ischemia after transplantation and provides better environments.

The cause of reduction in the graft size during the 8 weeks after the cell-sheet transplantation in both groups was not fully addressed in this study. However, one may consider that this reduction was caused by host immune rejection. We used a combined 3 immunosuppressant regimen, consisting of tacrolimus, mycophenolate mofetil, and corticosteroid, because our experiment was a xenotransplantation model, in which human tissue–derived cells were transplanted in a porcine. In addition, mesenchymal stem cells, which have the potential to induce immunologic tolerance,[29] were involved in creating hiPS-CM cell sheets, and recent studies have reported that the omentum has not only angiogenic cytokines and growth factors but also anti-inflammatory properties and thus can facilitate tissue healing of injured tissue or organs.[30] With our cell delivery method that combines the cell-sheet method with the pedicled omental flap, the 3-drug immunosuppressant regimen, and a mixture of mesenchymal stem cells, it would be difficult to permanently maintain a large number of delivered cells in this xenotransplantation model. Future clinical study of hiPS-CM transplantation for treating heart disease might be performed as allogeneic transplantation.[31] Further studies related to immunologic tolerance are needed to maintain the delivered cells long-term or permanently in this treatment.

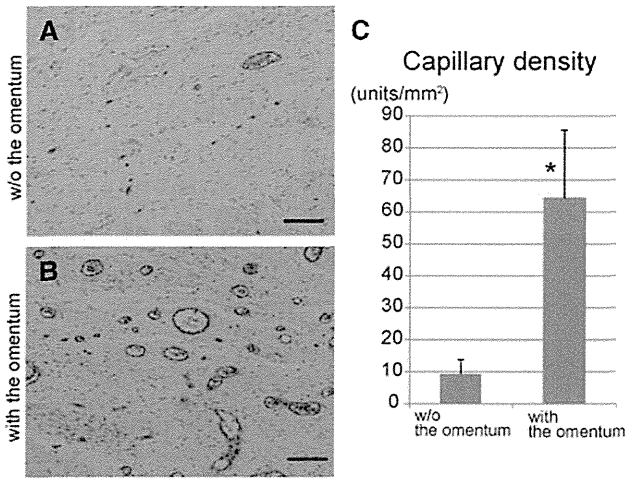

Figure 5. Capillary density in the transplanted area. Photomicrographs of immunostaining for von Willebrand factor are shown in **A** and **B**; scale bar, 50 μm. **C**, The capillary density in the transplanted area was significantly greater in the mini-pigs with the omentum than in those without it. *P<0.0001 vs without the omentum.

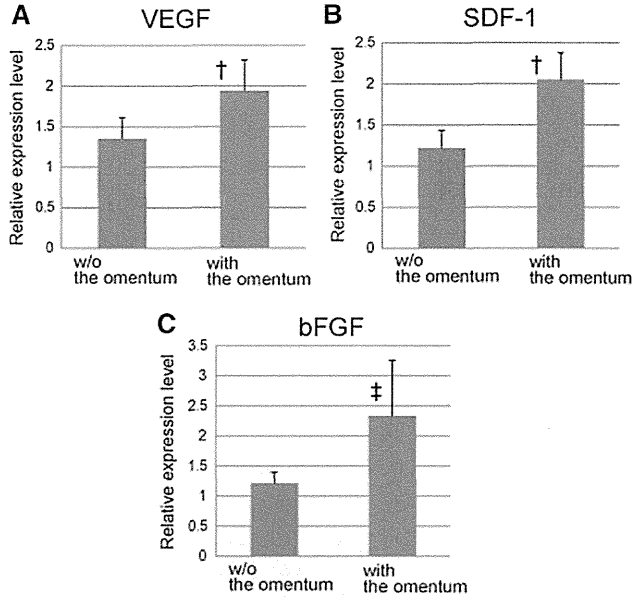

Figure 6. Angiogenesis-related mRNA expression in the transplanted area, as measured by real-time polymerase chain reaction. Relative expression of angiogenesis-related factors at the transplanted area was significantly greater in mini-pigs with the omentum than in those without it (**A**, vascular endothelial growth factor [VEGF], †P<0.05; **B**, stromal-derived factor [SDF]-1, †P<0.05; **C**, basic fibroblast growth factor [bFGF], ‡P<0.01 vs without the omentum).

In addition, more importantly, hiPS-CM cell sheets were transplanted over the normal epicardium, in which the tissue structure is well organized. New vascular network formation between the native myocardium and the transplanted cell sheets is thus insufficient to support the survival of the transplanted cells, leading to reduction of surviving transplanted cells long-term. In the clinical scenario, however, cell sheets will be transplanted over the diseased heart surface, in which epicardial structure is impaired. Conditions of the host myocardium possibly influence the survival of the transplanted cells. Our results indicate that transplanted cell sheets may provide sufficient blood supply, not from the host myocardium but from the omentum tissue. Thus, we consider that the omentum flap technique could provide a well-organized vascular network, regardless of conditions of the host myocardium, to enhance the survival of the transplanted cells. Further studies are needed to explore the mechanisms underlying integration of the transplanted cells sheets into the heart and to develop methods to enhance the survival and functionality of the transplanted cells.

Cardiac tissue engineering is another strategy that uses stem cells for the treatment of heart failure. One of the major challenges of in vitro engineering techniques is to overcome the limited thickness of the construct because the maximum oxygen diffusion is limited to ≈200 μm². A few recent methodologies have successfully yielded thicker engineered cardiac tissues. Cardiomyocytes in the Matrigel matrix were implanted with an arteriovenous blood vessel loop in vivo, and spontaneously contracting, thick, 3-dimensional constructs with extensive vascularization were thus attained.[32] The cell-sheet method, which is a scaffold-free system, is also an in vitro engineering technique. A cell sheet, itself, has a potential to induce angiogenesis quickly after implantation, and cell-dense 1-mm thick cardiac tissue was developed by repeated transplantation of triple-layered rat neonatal cardiac cell sheets.[33] This cardiac graft generated by this method, however, would be limited in use as a graft transplanted to the heart because of the lack of responsible large arteries and veins that can be revascularized after transplantation to the heart. In the present study, we used the omentum as a blood supply source after cell transplantation and demonstrated that the omentum enhanced angiogenesis and survival of the delivered cells. In addition, the omentum can easily be handled and mobilized, preserving its vascular network. The omentum, therefore, is a promising tool for in vivo vascularization in cardiac tissue engineering, although further studies with technological development would be needed for this strategy.

In conclusion, covering of the omentum flap over the transplanted hiPS-CM cell sheets on the myocardium effectively promoted angiogenesis, leading to enhanced survival of the hiPS-CMs. These results warrant further investigations as a clinically relevant strategy to enhance hiPS-CM transplantation therapy for heart failure.

Acknowledgments

We thank Shigeru Matsumi, Yuka Fujiwara, Hiromi Nishinaka, and Akima Harada for their excellent technical assistance.

Sources of Funding

This work was supported by the Japan Society for the Promotion of Science Core-to-Core Program and the Highway Program for the Realization of Regenerative Medicine of the Japanese Ministry of Education Sports, Science, and Technology.

Disclosures

Dr Shimizu is a consultant for CellSeed, Inc. Dr Okano is an Advisory Board Member in CellSeed, Inc, and an inventor/developer designated on the patent for temperature -responsive culture surfaces. The other authors report no conflicts.

References

1. Menasche P. Cardiac cell therapy: lessons from clinical trials. *J Mol Cell Cardiol*. 2011;50:258–265.
2. Hsiao LC, Carr C, Chang KC, Lin SZ, Clarke K. Stem cell-based therapy for ischemic heart disease. *Cell Transplant*. 2013;22:663–675.
3. Chimenti I, Smith RR, Li TS, Gerstenblith G, Messina E, Giacomello A, Marbán E. Relative roles of direct regeneration versus paracrine effects of human cardiosphere-derived cells transplanted into infarcted mice. *Circ Res*. 2010;106:971–980.
4. Tang XL, Rokosh G, Sanganalmath SK, Yuan F, Sato H, Mu J, Dai S, Li C, Chen N, Peng Y, Dawn B, Hunt G, Leri A, Kajstura J, Tiwari S, Shirk G, Anversa P, Bolli R. Intracoronary administration of cardiac progenitor cells alleviates left ventricular dysfunction in rats with a 30-day-old infarction. *Circulation*. 2010;121:293–305.
5. Takahashi K, Tanabe K, Ohnuki M, Narita M, Ichisaka T, Tomoda K, Yamanaka S. Induction of pluripotent stem cells from adult human fibroblasts by defined factors. *Cell*. 2007;131:861–872.
6. Yu J, Vodyanik MA, Smuga-Otto K, Antosiewicz-Bourget J, Frane JL, Tian S, Nie J, Jonsdottir GA, Ruotti V, Stewart R, Slukvin II, Thomson JA. Induced pluripotent stem cell lines derived from human somatic cells. *Science*. 2007;318:1917–1920.
7. Yoshida Y, Yamanaka S. iPS cells: a source of cardiac regeneration. *J Mol Cell Cardiol*. 2011;50:327–332.
8. Shimizu T, Yamato M, Isoi Y, Akutsu T, Setomaru T, Abe K, Kikuchi A, Umezu M, Okano T. Fabrication of pulsatile cardiac tissue grafts using a novel 3-dimensional cell sheet manipulation technique and temperature-responsive cell culture surfaces. *Circ Res*. 2002;90:e40.
9. Zvibel I, Smets F, Soriano H. Anoikis: roadblock to cell transplantation? *Cell Transplant*. 2002;11:621–630.
10. Memon IA, Sawa Y, Fukushima N, Matsumiya G, Miyagawa S, Taketani S, Sakakida SK, Kondoh H, Aleshin AN, Shimizu T, Okano T, Matsuda H. Repair of impaired myocardium by means of implantation of engineered autologous myoblast sheets. *J Thorac Cardiovasc Surg*. 2005;130:1333–1341.
11. Sekine H, Shimizu T, Dobashi I, Matsuura K, Hagiwara N, Takahashi M, Kobayashi E, Yamato M, Okano T. Cardiac cell sheet transplantation improves damaged heart function via superior cell survival in comparison with dissociated cell injection. *Tissue Eng Part A*. 2011;17:2973–2980.
12. Sawa Y, Miyagawa S, Sakaguchi T, Fujita T, Matsuyama A, Saito A, Shimizu T, Okano T. Tissue engineered myoblast sheets improved cardiac function sufficiently to discontinue LVAS in a patient with DCM: report of a case. *Surg Today*. 2012;42:181–184.
13. Kawamura M, Miyagawa S, Miki K, Saito A, Fukushima S, Higuchi T, Kawamura T, Kuratani T, Daimon T, Shimizu T, Okano T, Sawa Y. Sheets in a porcine ischemic cardiomyopathy model. *Circulation*. 2012;126:S29–S37.
14. O'Shaugnessy L. Surgical treatment of cardiac ischemia. *Lancet*. 1937;232:185–94.
15. Bigelow WG, Basian H, Trusler GA. Internal mammary artery implantation for coronary heart disease. A clinical follow-up study on to eight years after operation. *J Thorac Cardiovasc Surg*. 1963;45:67–79.
16. Aldridge HE, Macgregor DC, Lansdown EL, Bigelow WG. Internal mammary artery implantation for the relief of angina pectoris: a follow-up study of 77 patients for up to 13 years. *Can Med Assoc J*. 1968;98:194–198.
17. Shrager JB, Wain JC, Wright CD, Donahue DM, Vlahakes GJ, Moncure AC, Grillo HC, Mathisen DJ. Omentum is highly effective in the management of complex cardiothoracic surgical problems. *J Thorac Cardiovasc Surg*. 2003;125:526–532.
18. Takaba K, Jiang C, Nemoto S, Saji Y, Ikeda T, Urayama S, Azuma T, Hokugo A, Tsutsumi S, Tabata Y, Komeda M. A combination of omental flap and growth factor therapy induces arteriogenesis and increases myocardial perfusion in chronic myocardial ischemia: evolving concept of biologic coronary artery bypass grafting. *J Thorac Cardiovasc Surg*. 2006;132:891–899.
19. Shudo Y, Miyagawa S, Fukushima S, Saito A, Shimizu T, Okano T, Sawa Y. Novel regenerative therapy using cell-sheet covered with omentum flap delivers a huge number of cells in a porcine myocardial infarction model. *J Thorac Cardiovasc Surg*. 2011;142:1188–1196.
20. Toyoda K, Tooyama I, Kato M, Sato H, Morikawa S, Hisa Y, Inubushi T. Effective magnetic labeling of transplanted cells with HVJ-E for magnetic resonance imaging. *Neuroreport*. 2004;15:589–593.
21. Miyoshi S, Flexman JA, Cross DJ, Maravilla KR, Kim Y, Anzai Y, Oshima J, Minoshima S. Transfection of neuroprogenitor cells with iron nanoparticles for magnetic resonance imaging tracking: cell viability, differentiation, and intracellular localization. *Mol Imaging Biol*. 2005;7:286–295.
22. Kraitchman DL, Heldman AW, Atalar E, Amado LC, Martin BJ, Pittenger MF, Hare JM, Bulte JW. *In vivo* magnetic resonance imaging of mesenchymal stem cells in myocardial infarction. *Circulation*. 2003;107:2290–2293.
23. Takehara N, Tsutsumi Y, Tateishi K, Ogata T, Tanaka H, Ueyama T, Takahashi T, Takamatsu T, Fukushima M, Komeda M, Yamagishi M, Yaku H, Tabata Y, Matsubara H, Oh H. Controlled delivery of basic fibroblast growth factor promotes human cardiosphere-derived cell engraftment to enhance cardiac repair for chronic myocardial infarction. *J Am Coll Cardiol*. 2008;52:1858–1865.
24. Mangi AA, Noiseux N, Kong D, He H, Rezvani M, Ingwall JS, Dzau VJ. Mesenchymal stem cells modified with Akt prevent remodeling and restore performance of infarcted hearts. *Nat Med*. 2003;9:1195–1201.
25. Li W, Ma N, Ong LL, Nesselmann C, Klopsch C, Ladilov Y, Furlani D, Piechaczek C, Moebius JM, Lützow K, Lendlein A, Stamm C, Li RK, Steinhoff G. Bcl-2 engineered MSCs inhibited apoptosis and improved heart function. *Stem Cells*. 2007;25:2118–2127.
26. Tulloch NL, Muskheli V, Razumova MV, Korte FS, Regnier M, Hauch KD, Pabon L, Reinecke H, Murry CE. Growth of engineered human myocardium with mechanical loading and vascular coculture. *Circ Res*. 2011;109:47–59.
27. Matsuura K, Wada M, Shimizu T, Haraguchi Y, Sato F, Sugiyama K, Konishi K, Shiba Y, Ichikawa H, Tachibana A, Ikeda U, Yamato M, Hagiwara N, Okano T. Creation of human cardiac cell sheets using pluripotent stem cells. *Biochem Biophys Res Commun*. 2012;425:321–327.
28. Yu T, Miyagawa S, Miki K, Saito A, Fukushima S, Higuchi T, Kawamura M, Kawamura T, Ito E, Kawaguchi N, Sawa Y, Matsuura N. *In vivo* differentiation of induced pluripotent stem cell-derived cardiomyocytes. *Circ J*. 2013;77:1297–1306.
29. Uccelli A, Moretta L, Pistoia V. Mesenchymal stem cells in health and disease. *Nat Rev Immunol*. 2008;8:726–736.
30. Chandra A, Srivastava RK, Kashyap MP, Kumar R, Srivastava RN, Pant AB. The anti-inflammatory and antibacterial basis of human omental defense: selective expression of cytokines and antimicrobial peptides. *PLoS One*. 2011;6:e20446.
31. Pearl JI, Lee AS, Leveson-Gower DB, Sun N, Ghosh Z, Lan F, Ransohoff J, Negrin RS, Davis MM, Wu JC. Short-term immunosuppression promotes engraftment of embryonic and induced pluripotent stem cells. *Cell Stem Cell*. 2011;8:309–317.
32. Morritt AN, Bortolotto SK, Dilley RJ, Han X, Kompa AR, McCombe D, Wright CE, Itescu S, Angus JA, Morrison WA. Cardiac tissue engineering in an *in vivo* vascularized chamber. *Circulation*. 2007;115:353–360.
33. Shimizu T, Sekine H, Yang J, Isoi Y, Yamato M, Kikuchi A, Kobayashi E, Okano T. Polysurgery of cell sheet grafts overcomes diffusion limits to produce thick, vascularized myocardial tissues. *FASEB J*. 2006;20:708–710.

Circulation
JOURNAL OF THE AMERICAN HEART ASSOCIATION

American Heart Association®

Spatially Oriented, Temporally Sequential Smooth Muscle Cell-Endothelial Progenitor Cell Bi-Level Cell Sheet Neovascularizes Ischemic Myocardium

Yasuhiro Shudo, Jeffrey E. Cohen, John W. MacArthur, Pavan Atluri, Philip F. Hsiao, Elaine C. Yang, Alexander S. Fairman, Alen Trubelja, Jay Patel, Shigeru Miyagawa, Yoshiki Sawa and Y. Joseph Woo

Circulation. 2013;128:S59-S68
doi: 10.1161/CIRCULATIONAHA.112.000293
Circulation is published by the American Heart Association, 7272 Greenville Avenue, Dallas, TX 75231

Print ISSN: 0009-7322. Online ISSN: 1524-4539

Spatially Oriented, Temporally Sequential Smooth Muscle Cell-Endothelial Progenitor Cell Bi-Level Cell Sheet Neovascularizes Ischemic Myocardium

Yasuhiro Shudo, MD, FAHA; Jeffrey E. Cohen, MD; John W. MacArthur, MD; Pavan Atluri, MD, FAHA; Philip F. Hsiao, BA; Elaine C. Yang, MS; Alexander S. Fairman, BA; Alen Trubelja, BS; Jay Patel, BS; Shigeru Miyagawa, MD, PhD; Yoshiki Sawa, MD, PhD; Y. Joseph Woo, MD, FAHA

Background—Endothelial progenitor cells (EPCs) possess robust therapeutic angiogenic potential, yet may be limited in the capacity to develop into fully mature vasculature. This problem might be exacerbated by the absence of a neovascular foundation, namely pericytes, with simple EPC injection. We hypothesized that coculturing EPCs with smooth muscle cells (SMCs), components of the surrounding vascular wall, in a cell sheet will mimic the native spatial orientation and interaction between EPCs and SMCs to create a supratherapeutic angiogenic construct in a model of ischemic cardiomyopathy.

Methods and Results—Primary EPCs and SMCs were isolated from Wistar rats. Confluent SMCs topped with confluent EPCs were spontaneously detached from the Upcell dish to create an SMC-EPC bi-level cell sheet. A rodent ischemic cardiomyopathy model was created by ligating the left anterior descending coronary artery. Rats were then immediately divided into 3 groups: cell-sheet transplantation (n=14), cell injection (n=12), and no treatment (n=13). Cocultured EPCs and SMCs stimulated an abundant release of multiple cytokines in vitro. Increased capillary density and improved blood perfusion in the borderzone elucidated the significant in vivo angiogenic potential of this technology. Most interestingly, however, cell fate–tracking experiments demonstrated that the cell-sheet EPCs and SMCs directly migrated into the myocardium and differentiated into elements of newly formed functional vasculature. The robust angiogenic effect of this cell sheet translated to enhanced ventricular function as demonstrated by echocardiography.

Conclusions—Spatially arranged EPC-SMC bi-level cell-sheet technology facilitated the natural interaction between EPCs and SMCs, thereby creating structurally mature, functional microvasculature in a rodent ischemic cardiomyopathy model, leading to improved myocardial function. (***Circulation.* 2013;128[suppl 1]:S59–S68.)**

Key Words: angiogenesis ■ cardiovascular diseases ■ cells ■ endothelium ■ heart failure ■ tissue

Heart failure is the leading cause of death in the United States, with a 5-year mortality of 50%. Current treatment for heart failure entails medical optimization, along with limited revascularization and reconstructive techniques. These interventions do not address the microvascular deficiencies that develop in ischemic cardiomyopathy (ICM). Myocardial regenerative and cellular therapy is attracting growing interest as a means to improve left ventricular (LV) function in advanced heart failure. Among the many candidate cells, endothelial progenitor cells (EPCs), the precursor of blood vessels, have demonstrated excellent potential for therapeutic angiogenesis. Recent reports show beneficial effects of EPC transplantation therapy in several animal experimental models and patients with heart failure.[1–3]

The mechanism by which damaged myocardium is restored by transplanted EPCs is complex and involves many pathways. Recent large-scale clinical trials, in which EPCs were delivered using direct myocardial injection[4] or catheter-based intracoronary procedures,[5,6] reported only modest therapeutic benefits. The limited benefits are at least partially because of poor localized cell survival after transplantation, thereby greatly attenuating the angiogenic potential of EPC therapy. In addition, mature vasculature requires the presence of supporting elements, such as smooth muscle cells (SMCs), which are not delivered with simple EPC injection. In contrast, cell-sheet technology delivers cells more effectively with minimal cell dispersion and myocardial injury and improves microvascular structure, leading to better cardiac function than that attained

From the Division of Cardiovascular Surgery, Department of Surgery, University of Pennsylvania School of Medicine, Philadelphia, PA (Y.S., J.E.C., J.W.M., P.A., P.F.H., E.C.Y., A.S.F., A.T., J.P., Y.J.W.); and Department of Cardiovascular Surgery, Osaka University Graduate School of Medicine, Osaka, Japan (S.M., Y.S.).

Presented at the American Heart Association meeting in Los Angeles, CA, November 3–7, 2012.

This article was handled independently by Frank Sellke, MD, as a Guest Editor.

Correspondence to Y. Joseph Woo, MD, Division of Cardiovascular Surgery, Department of Surgery, University of Pennsylvania School of Medicine, 3400 Spruce St, 6 Silverstein, Philadelphia, PA 19104. E-mail wooy@uphs.upenn.edu

Circulation **is available at http://circ.ahajournals.org** **DOI: 10.1161/CIRCULATIONAHA.112.000293**

by intracoronary injection or needle injection.[7–11] Specifically, the cell-sheet technology enables the construction of a cellular system that mimics the natural architecture of a desired tissue. Here, the proposed angiogenic therapy uses the cell sheet to optimize the spatial arrangement of EPCs and SMCs to maximally induce structurally mature vasculature. The cell sheet is generated on and removed from special dishes that are grafted with a temperature-responsive polymer that changes from hydrophobic to hydrophilic when the temperature is lowered. The greatest advantage of this technique is that the cell sheet consists of densely adherent cells without requiring an artificial scaffold, it is easily manipulated and has a high ability to integrate with native tissues without destroying the cell–cell or cell–extracellular matrix (ECM) adhesions in the cell sheet.[7] In addition, we focused on the concept that the natural endothelial–pericyte spatial relationship and interaction are crucial for vessel maturation and stabilization. Thus, we hypothesized that SMCs, which are components of vascular pericytes, would enhance EPC-mediated angiogenesis and facilitate blood vessel maturation. Neoangiogenesis should yield increased blood perfusion and restoration of cardiomyocyte viability. To demonstrate clear and direct contribution of the cell-sheet EPCs and SMCs to neovasculature, we constructed multiple fate-tracking experiments. A labeled cell sheet was created with EPCs from female rats ubiquitously expressing the enhanced green fluorescent protein (GFP), along with SMCs from male rats. This cell sheet with trackable elements was then implanted in female rats.

In short, this study examined the functional benefits of transplanting the bi-level cell sheet created from cocultured EPCs and SMCs in an ICM model, compared with direct myocardial needle injection.

Methods

Isolation of EPCs and SMCs

Wistar rats were administered pentobarbital (100 mg/kg, IP), and then the carotid artery was dissected and transected. Bone marrow mononuclear cells were isolated from the long bones of rats by density gradient centrifugation with Histopaque 1083 (Sigma-Aldrich) and cultured in endothelial basal medium-2 supplemented with EGM-2 SingleQuot (Lonza) containing human epidermal growth factor, 5% fetal bovine serum (Sigma-Aldrich), vascular endothelial growth factor (VEGF), basic human fibroblast growth factor, recombinant human long R3 insulin-like growth factor-1, ascorbic acid, gentamicin, and amphotericin B. The combination of endothelium-specific media and the removal of nonadherent bone marrow mononuclear cells were intended to select for the EPC phenotype. EPCs were cultured for 7 days in the same medium.[2] For EPC fate tracking, we used GFP transgenic female Wistar rats.

SMCs were isolated from the thoracic aorta of wild-type male Wister rats (3 weeks old; Charles River) by primary explant technique[12] and cultured in DMEM with 20% fetal bovine serum, gentamicin, and amphotericin B to confluency for 7 days at 37°C and 5% CO_2. For SMC fate tracking, we used male Wistar rats.

Bi-Level Cell-Sheet Preparation

The SMCs were plated at 1.5×10^5/cm^2 in a 35-mm Upcell dish, which is grafted with temperature-responsive polymers (CellSeed, Tokyo, Japan), and then cultured in EPC-specific medium. After 24 hours of culture at 37°C and 5% CO_2, EPCs were added at 1.5×10^5/cm^2 onto the Upcell dish, which was already confluent with SMCs. After 24 additional hours in culture, the dishes were transferred to another incubator, set at 20°C, for 1 hour to release the cultured cells as an intact cell sheet. Under this protocol, confluent SMCs topped with confluent EPCs were spontaneously detached from the plate as a sequentially cocultured and specifically spatially oriented SMC-EPC bi-level cell sheet (Figure 1A).[10,11]

Production and Release of Cytokines/Chemokines

To demonstrate proangiogenic biological activity, supernatant of the cocultured cells (EPCs: 1.5×10^5/cm^2, SMCs: 1.5×10^5/cm^2), EPCs (3.0×10^5/cm^2), or SMCs (3.0×10^5/cm^2), after being cultured for 24 hours, was centrifuged to remove debris and contaminating cells. Levels of VEGF, hepatocyte growth factor (HGF), transforming growth factor-β (TGFβ), and stromal cell–derived factor 1α (SDF1α) in the culture supernatants were analyzed by ELISA kit (Quantikine, R&D Minneapolis, MN; n=6 in each). ELISA was performed in duplicate.

Assessment of Cytokine Receptor Expressions by Flow Cytometry

To elucidate the biological impact of cocultured EPCs and SMCs on fetal liver kinase 1 (FLK1) and VEGF receptor 2 (VEGFR2) expression, flow cytometry was used in the EPC or SMC cultured with SMC or EPC using the transwell inserts, supplemented with recombinant VEGF, or media only for 24 hours (n=5 in each). The amount of VEGF was determined based on the results of ELISA. Test samples were incubated for 1 hour at room temperature with either mouse monoclonal anti-FLK1 (Santa Cruz Biotechnology) or rabbit anti-VEGFR2 (Abcam). After washing with cold fluorescence-activated cell sorter buffer, cells were incubated at room temperature

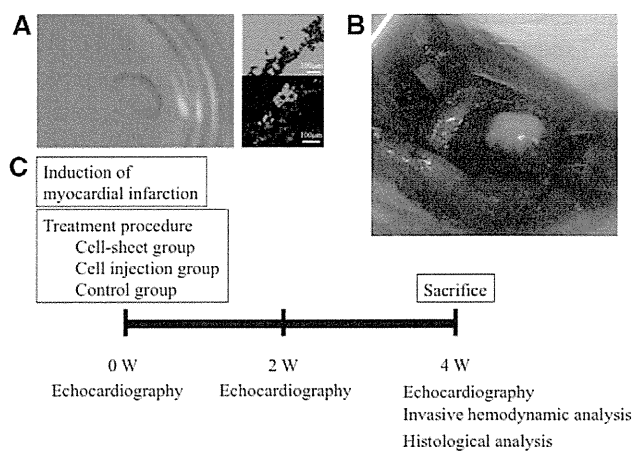

Figure 1. Preparation and transplantation of bi-level cocultured cell-sheet containing both endothelial progenitor cells (EPCs) and smooth muscle cells (SMCs). **A**, Confluent SMCs topped with confluent EPCs were spontaneously detached from an Upcell dish, which is grafted with temperature-responsive polymers (CellSeed, Tokyo, Japan), as a sequentially cocultured and specifically spatially oriented SMC-EPC bi-level cocultured cell-sheet. Hematoxylin-eosin staining; cross-sectional views of cell-sheet in vitro. Cocultured bi-level cell sheet maintained green fluorescent protein (GFP)-positive EPCs and Y chromosome–positive SMCs in separate layers in vitro. Red indicates rat Y chromosome; green, GFP. **B**, Bi-level cocultured cell-sheet, which consisted of 1.3×10^6 EPCs and 1.3×10^6 SMCs, was placed into the epicardium of the left ventricle covering the ischemic area. **C**, Study protocol used for assessment of cardiac function and histology. Wistar rats underwent induction of myocardial infarction by occluding the LAD permanently, followed by the concurrent treatment procedure. Cardiac function was assessed by echocardiography just before and at 2 and 4 weeks after the treatment procedure. Four weeks after the treatment procedure, invasive hemodynamic analysis and histological examination were performed after euthanasia.

for 30 minutes with Alexa 647 chicken anti-mouse IgG (Invitrogen) and Alexa 488 donkey anti-rabbit IgG (Invitrogen). The percentage of cells expressing each cell surface antigen was analyzed with a Becton Dickinson FACSCalibur flow cytometer. Data analysis was performed using FlowJo 8.8.3 (Tree Star Inc).[3,13]

Rat ICM Model and Cell-Sheet Transplantation

Female Wistar rats (8 weeks old, 250–300g; Charles River) were anesthetized with ketamine (75 mg/kg IP) and xylazine (7.5 mg/kg IP), intubated in an endotracheal manner with a 19-gauge catheter, and mechanically ventilated (Hallowell EMC). Anesthesia was maintained by inhalation of 2.0% isoflurane (Clipper Distributing Company Llc, Saint Joseph, MO).

The proximal left anterior descending coronary artery (LAD) of Wistar rats was permanently occluded using a left thoracotomy approach. This produced a consistent and reproducible myocardial infarction encompassing 35% to 40% of the left ventricle.[1–3] Within 5 minutes after LAD ligation, the rats were allocated into 3 groups by simple randomization, considering that there were no differences among the animals at this time point: those that underwent cocultured cell-sheet transplantation (cell-sheet group, n=14), those that underwent cocultured cell injection (cell injection group, n=12), and those that underwent no intervention (control group, n=13). The rats were allowed to recover under care.

In the cell-sheet group, the cocultured bi-level cell sheet, which consists of 1.3×10^6 EPCs and 1.3×10^6 SMCs, was placed on the epicardium covering the ischemic area (Figure 1B). The cell injection group received 1.3×10^6 EPCs and 1.3×10^6 SMCs, diluted in saline for a total volume of 200 μL by direct intramyocardial injection with a 30-gauge needle. Each rat received the same number of cells. Animals were then kept in temperature-controlled individual cages for 4 weeks.

The rats were euthanized at 4 weeks after surgery by intravenous injection of 200 mg/kg of pentobarbital and 2 mEq/kg of potassium chloride, under terminal anesthesia, and the heart was excised.

Histological and Immunohistochemical Analyses

Four weeks after treatment, the hearts were dissected and embedded in optimum cutting temperature compound for 10-μm-thick cryosections. The cryosections were used for routine hematoxylin-eosin staining to assess the myocardial structure. Masson trichrome staining was performed to assess cardiac fibrosis in the peri-infarct borderzone. The fibrotic region was calculated as the percentage of myocardial area. The data were collected from 5 individual views per heart at a magnification of ×200. The heart cryosections were also stained with an antibody to von Willebrand factor (vWF; 1:200 dilution; Abcam) to assess capillary density, which was calculated as the number of positively stained capillary vessels in 5 randomly selected fields in the peri-infarct borderzone area, per heart. The cryosections were also stained with an antibody to proliferating cell nuclear antigen (1:200 dilution; Abcam) to assess cellular proliferative activity in 5 randomly selected fields in the peri-infarct borderzone area. The cryosections were also stained with an antibody to integrin β1 (1:100 dilution; Abcam) to estimate cell–matrix attachment in 5 randomly selected fields in the peri-infarct borderzone area. Cell nuclei were counterstained with 6-diamidino-2-phenylindole (Invitrogen). The images were examined by fluorescence microscopy (Leica). Image J software was used for quantitative morphometric analysis.

EPC-SMC Fate Tracking

The cell sheet, which consisted of EPCs from GFP transgenic female Wistar rats and SMCs from non-GFP male Wistar rats, was transplanted into the female Wistar rat heart. To detect the fate of EPCs, cryosections were stained with an anti-vWF antibody (1:1000 dilution; Abcam), anti–smooth muscle actin (SMA) antibody (1:1000 dilution; Abcam), anti–vascular endothelial-cadherin antibody (1:1000 dilution; Santa Cruz), and anti-GFP antibody (1:1000 dilution; Abcam). The secondary antibodies were Alexa Fluor 555 donkey anti-rabbit IgG (1:1000 dilution; Invitrogen) and Alexa Fluor 555 donkey anti-mouse IgG (1:1000 dilution; Invitrogen). To detect the fate of SMCs, fluorescence in situ hybridization was performed on cryosections, which were then stained with anti-SMA antibody (1:500 dilution; Abcam). The secondary antibody was Alexa Fluor 555 donkey anti-rabbit IgG (1:500 dilution; Invitrogen). Cell nuclei were counterstained with 6-diamidino-2-phenylindole. GFP-positive cells and rat Y chromosome–positive cells were counted, respectively, and corrected by total number of tissue cells to estimate the survival cells quantitatively. GFP- and vWF-positive cells were counted and corrected by total number of GFP-positive cells to examine vascular regeneration. Rat Y chromosome– and SMA-positive cells were counted and corrected by total number of rat Y chromosome–positive cells to examine vascular regeneration.

Myocardial Perfusion Analysis

To quantify myocardial perfusion, at 4 weeks after treatment 200 μg of fluorescein-labeled *Lycopersicon esculentum* (tomato) lectin (Vector Laboratories) was injected into the supradiaphragmatic inferior vena cava and allowed to circulate for 10 minutes. After lectin perfusion, the hearts were explanted and snap-frozen in liquid nitrogen. One-hundred twenty sequential images were obtained through 100-μm thick myocardial sections at the level of the papillary muscle using scanning laser confocal microscopy (z-series, ×20 air magnification, Zeiss LSM-510 Meta Confocal Microscope). Three-dimensional reconstructions of the image stacks were created using Velocity Software v.3.61 (Improvision). Fluorescein-labeled voxels were quantified as a percentage of total tissue section voxels, creating a quantifiable measurement of perfusion per unit of myocardial tissue volume.[2,3]

Echocardiographic Assessment

Echocardiography was performed under general anesthesia using 1.0% inhaled isoflurane just before and at 2 and 4 weeks after the treatment procedure (SONOS 7500, Philips Medical Systems, Andover, MA) with a 12-MHz transducer at an image depth of 2 cm (cell sheet, n=7; cell injection, n=8; control, n=9; Figure 1C). LV end-diastolic diameter (LVEDD), LV end-systolic diameter (LVESD), and end-diastolic anterior wall thickness at the level of the papillary muscles were measured for ≥3 consecutive cardiac cycles following the American Society for Echocardiology leading-edge method. Fractional shortening (FS) and ejection fraction (EF) were calculated as parameters of systolic function.[2,3,8] All analyses were performed by a single investigator in a group-blinded fashion.

Invasive Hemodynamic Assessment

Four weeks after the treatment procedure, animals (cell-sheet, n=6; cell injection, n=6; control, n=8) underwent invasive hemodynamic measurements with a pressure–volume conductance catheter (SPR-869; Millar Instruments, Inc; Figure 1C). The catheter was calibrated via 5-point cuvette linear interpolation with parallel conductance subtraction by the hypertonic saline method.[2,3] Rats were anesthetized using 1.0% inhaled isoflurane, and the catheter was introduced into the LV with a closed-chest approach via the right carotid artery. Measurements were obtained before and during inferior vena cava occlusion to produce static and dynamic pressure–volume loops under varying load conditions. Data were recorded and analyzed with LabChart version 6 software (AD Instruments) and ARIA Pressure Volume Analysis software (Millar Instruments, Inc). After hemodynamic assessment, the heart was removed for further histological analyses.

Statistical Analysis

Continuous variables are expressed as mean±SE. Comparisons between 2 groups were made using the Wilcoxon–Mann–Whitney *U* test because of small sample sizes. For comparisons among 3 groups, we used the Kruskal–Wallis test, followed by the post hoc pairwise Wilcoxon–Mann–Whitney *U* test. The multiplicity in pairwise comparisons was corrected by the Bonferroni procedure. A $P<0.05$ was

considered statistically significant. All statistical calculations were performed using SPSS software (version 11.0; SPSS Inc, Chicago, IL) and JMP 9.0 (SAS Institute Inc, Cary, NC).

Animal Care and Biosafety

Wistar rats were obtained from Charles River. Food and water were provided ad libitum. This investigation conforms with the Guide for the Care and Use of Laboratory Animals published by the US National Institutes of Health (NIH Publication No. 85-23, revised 1996) and was approved by the Institutional Animal Care and Use Committee of the University of Pennsylvania (protocol 803394).

Results

Production and Release of Cytokines/Chemokines by Coculturing EPC With SMC

VEGF was significantly higher in the coculture supernatant than the SMC-only group and tended to be higher than the EPC-only group (Figure 2A). The secretion of HGF was remarkably enhanced in the coculture supernatant, whereas HGF levels were not evident in either the EPC- or SMC-alone group (Figure 2B). The concentration of TGFβ was significantly higher in the coculture supernatant than both the EPC- and SMC-only groups (Figure 2C). The secretion of SDF1α was remarkably higher in the cocultured group compared with EPC and SMC alone (Figure 2D).

Upregulated Expressions of FLK1 and VEGFR2 on Either EPC or SMC Under Cytokines-Rich Medium of SMC or EPC

Flow cytometric analysis demonstrated that the percentage of FLK1$^+$ EPCs and VEGFR2$^+$ EPCs in total EPC population was 1.3±0.3% and 3.2±0.8%, respectively. Supplementation with VEGF significantly increased the percentage of FLK1$^+$ EPCs (17.2±3.2%) and VEGFR2$^+$ EPCs (32.0±5.4%). Furthermore, the percentage of FLK1$^+$ and VEGFR2$^+$ EPCs was significantly greater after coculturing with SMC (FLK1$^+$, 39.6±9.2%; VEGFR2$^+$, 52.5±9.8%; Figure 3A and 3B).

Flow cytometric analysis demonstrated a statistically significant increase in the percentage of FLK1$^+$ SMCs cocultured with EPC compared with SMC alone (75.7±5.4 versus 23.9±2.5%; P=0.02). Addition of VEGF significantly increased FLK1$^+$ SMCs compared with SMC (Figure 3C and 3D). There was no significant difference in the VEGFR2$^+$ expression on SMCs (P=0.14, Kruskal–Wallis test).

Enhanced Capillary Density and Microvascular Perfusion After Cocultured Cell-Sheet Transplantation

A large number of vWF-positive blood vessels were detected in the peri-infarct borderzone myocardium after cell-sheet therapy compared with injection alone (Figure 4A). This demonstrated a superior enhancement of capillary density in the cell-sheet group (Figure 4B).

Similarly, lectin microangiography of the peri-infarct borderzone myocardium sections revealed a more densely and well-developed capillary network in the cell-sheet group compared with injection alone (Figure 4C). Quantitative analysis showed significantly enhanced perfusion in the peri-infarct borderzone myocardium in the cell-sheet group (Figure 4D).

Enhanced Cell Proliferation Activity After Cocultured Cell-Sheet Transplantation

A large number of proliferating cell nuclear antigen-positive cells were identified in the peri-infarct borderzone myocardium after cell-sheet therapy compared with control (Figure 4E and 4F).

Migration of EPCs and SMCs to Myocardium Contributing to Neovasculature

Cocultured bi-level cell sheet contained GFP-positive EPCs and Y chromosome–positive SMCs in separate layers in vitro (Figure 1A).

Four weeks after transplantation, the GFP-positive EPCs were detected in the myocardium at the transplanted site at an appropriate depth of 650 μm (Figure 4G). Immunostaining for vWF and GFP showed that transplanted EPCs were able to contribute to neovascularization of the host myocardium (Figure 4H). This was further supported by immunostaining for vascular endothelial-cadherin and GFP (Figure 4I). In addition, staining with antibody to SMA and GFP indicated that GFP-positive EPCs originating from the transplanted cocultured bi-level cell sheet migrated into the engineered

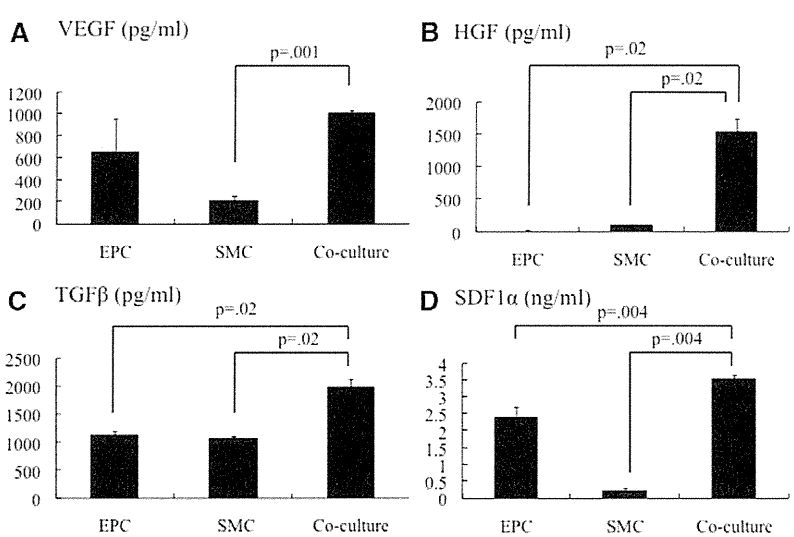

Figure 2. A, Vascular endothelial growth factor (VEGF), (**B**) hepatocyte growth factor (HGF), (**C**) transforming growth factor-β (TGFβ), and (**D**) stromal cell–derived factor 1α (SDF1α) in the culture supernatant, measured by ELISA. Cocultured endothelial progenitor cells (EPCs) with smooth muscle cells (SMCs) secreted abundant VEGF, HGF, TGFβ, and SDF1α compared with either EPC or SMC (n=6 in each; VEGF, P=0.002; HGF, P=0.01; TGFβ, P=0.01; SDF1α, P=0.001; Kruskal–Wallis test).

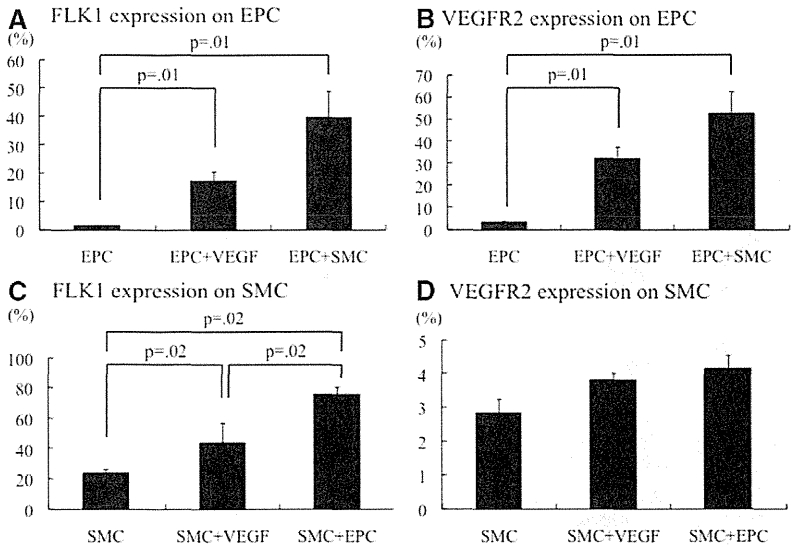

Figure 3. To elucidate the biological impact of cocultured endothelial progenitor cell (EPC)-smooth muscle cells (SMCs) on FLK1 and vascular endothelial growth factor receptor 2 (VEGFR2) expression, flow cytometry was used to study both EPC and SMC expression of these markers in the following settings: cocultured, cultured with VEGF, and cultured alone. The amount of VEGF used was determined based on the results of ELISA. **A** and **B**, The percentage of FLK1$^+$ EPC and VEGFR2$^+$ EPC was greatest in a cocultured setting (n=5 in each; FLK1 expression on EPC, P=0.01; VEGFR2 expression on EPC, P=0.01; Kruskal–Wallis test). **C** and **D**, Analysis of SMC FLK1$^+$ expression demonstrated a significant increase in the cocultured group. There was no significant difference in the VEGFR2$^+$ expression on SMC (n=4 in each; FLK1 expression on SMC, P=0.01; VEGFR2 expression on SMC, P=0.14; Kruskal–Wallis test).

myocardial tissues and were circumferentially surrounded by SMA-positive tissues (Figure 4J). Finally, to track SMCs from the cell sheet, we performed fluorescence in situ hybridization immediately to identify male SMCs in the female recipient. After the cell-sheet transplantation, GFP-positive EPCs and Y chromosome–positive SMCs were detected with a thickness of ≈50 μm into the epicardium (Figure 4K). Rat Y chromosome SMCs were partially able to differentiate into SMA-positive tissues (Figure 4L). Quantitative analysis showed a greater percentage of GFP-positive cells and rat Y chromosome–positive cells, respectively, in the cell-sheet group compared with cell injection (Figure 4M). Quantitative analysis of vascular regeneration showed that the number of both GFP- and vWF-positive cells is 18±3/hpf (60% of GFP-positive cells), which participated in new blood vessel formation. In addition, the number of both Y chromosome– and SMA-positive cells is 7±2/hpf (45% of rat Y chromosome cells), which participated in new blood vessel formation. One week after treatment, a large number of integrin β1–positive cells were observed in the peri-infarct borderzone myocardium after cell-sheet therapy compared with cell injection and control (Figure 4N and 4O).

LV Remodeling After Cell-Sheet Transplantation

The LV myocardial structure was superiorly maintained after cell-sheet transplantation compared with cell injection and control, as assessed by hematoxylin-eosin staining (Figure 5A). In addition, cell-sheet therapy significantly attenuated collagen accumulation in the infarct area compared with cell injection and control, as demonstrated by Masson trichrome staining (Figure 5B and 5C).

Cardiac Functional Recovery After Cell-Sheet Transplantation

The effects of cocultured bi-level cell-sheet transplantation on cardiac function were assessed in a rat ICM model. After permanent occlusion of the LAD, EF, FS, and anterior wall thickness (baseline, 1.7±0.1 mm; at 2 weeks, 0.8±0.1 mm, at 4 weeks, 0.8±0.1 mm; P=0.0001, Kruskal–Wallis test) showed steady reductions, whereas EDD/ESD showed steady increases (EDD, P=0.0002; ESD, P=0.0001; Kruskal–Wallis test), suggesting progressive LV remodeling. After cocultured cell injection, the heart showed mild recovery, including increases in FS and EF. At 4 weeks after treatment, EF and FS tended to be greater after cocultured cell injection than the control; however, an even greater recovery was observed after cell-sheet transplantation (Figure 6A and 6B). At 4 weeks, the bi-level cell-sheet group had a significantly greater EF and FS and significantly improved EDD and ESD compared with either cell injection or control (Figure 6C and 6D).

Assessment by pressure–volume catheter further confirmed the cell-sheet–induced functional enhancement demonstrated by the echocardiographic data. Four weeks after transplantation, the maximal rate of change in LV pressure (max. dP/dt) and end-systolic pressure–volume relationship were significantly enhanced in the cell-sheet group compared with cell injection and control (Figure 7). Mimimal rate of change in LV pressure (min. dP/dt) and cardiac output were higher in the cell-sheet group than the other 2 groups, but the difference was not significant.

Discussion

This study revealed a multifaceted mechanism by which the targeted implantation of an EPC-SMC bi-level cell-sheet enhances myocardial function in a rodent model of ICM. A significant chemokine effect was observed in vitro where cocultured EPC-SMCs stimulated an abundant release of SDF1α, VEGF, HGF, and TGFβ; this effect is a mechanistic component of the augmented angiogenesis demonstrated in vivo. More importantly, however, the data clearly established direct migration of the cell-sheet EPCs and SMCs into the myocardium and confirmed these cells to be some elements of newly formed functional vasculature. The observed increased capillary density and improved blood perfusion in the borderzone elucidated the significant in vivo angiogenic potential of this technology. Furthermore, cell fate–tracking experiments strongly suggested the cell-sheet EPCs and SMCs as components of newly assembled vasculature. With regard to cell engraftment, the cell-sheet group performed superiorly, demonstrating improved cell–matrix attachment compared

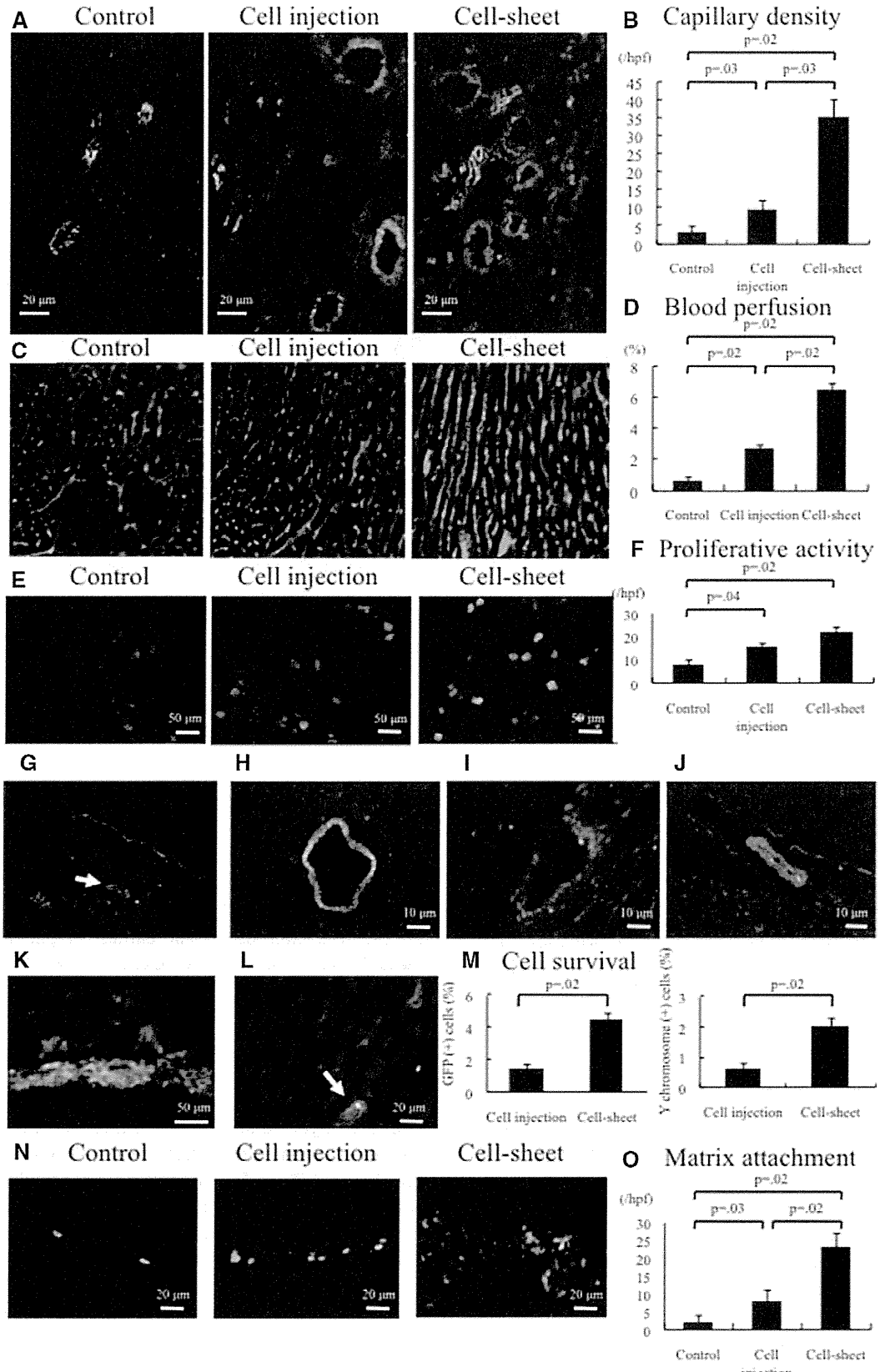

Figure 4. Effects on left ventricular remodeling, capillary density, and microvascular perfusion by bi-level cocultured cell-sheet transplantation (cell-sheet), cocultured cell injection (cell injection), and control (control) 4 weeks after the treatment procedure. **A**, Representative von Willebrand factor (vWF) staining of the borderzone myocardium. **B**, Quantification of capillary density. Capillary density was significantly enhanced in the cell-sheet groups compared with other groups (cell-sheet, n=4; cell injection, n=3; control, n=4; *P*=0.01, Kruskal–Wallis test). **C**, Representative lectin microangiographic imaging from the borderzone myocardium (×20 magnification). **D**, Quantitative analysis showed enhanced blood perfusion in the cell-sheet group compared with the other groups (cell sheet, n=4; cell injection, n=4; control, n=4; *P*=0.01, Kruskal–Wallis test). **E**, Representative antiproliferative cell nuclear

(*Continued*)

Figure 4. Continued antigen staining of the borderzone myocardium. **F**, Quantification of cell proliferative activity. Proliferative activity was significantly enhanced in the cell-sheet group compared with control (cell sheet, n=4; cell injection, n=4; control, n=4; *P*=0.02, Kruskal–Wallis test). **G**, Immunoconfocal microscopy demonstrated abundant green fluorescent protein (GFP)-positive cells in the myocardium. **H**, Cryosections were stained with an antibody to vWF and GFP to detect the fate of endothelial progenitor cells (EPCs) in the heart. Immunostaining for vWF and GFP showed that transplanted EPCs over the borderzone myocardium were able to contribute directly to neovascularization of the host myocardium. Green indicates GFP; red, vWF; blue, nuclei. **I**, Immunostaining for vascular endothelial (VE)-cadherin and GFP showed that transplanted EPCs were able to contribute to neovascularization of the host myocardium. Green indicates GFP; red, VE-cadherin; blue, nuclei. **J**, In addition, staining with antibody to smooth muscle actin (SMA) and GFP demonstrated that GFP-positive EPCs originating from the transplanted cocultured bi-level cell sheet migrated into the treated myocardial tissues and were circumferentially supported by SMA-positive tissues. Green indicates GFP; red, SMA; blue, nuclei. **K**, Furthermore, to track SMCs from the cell sheet, we performed fluorescence in situ hybridization to identify male SMCs in the female recipient. Immediately after the cell-sheet transplantation, GFP-positive EPCs and Y chromosome–positive SMCs were detected in the epicardium. Red indicates rat Y chromosome; green, GFP. **L**, Rat Y chromosome SMCs were able to differentiate into SMA-positive tissues (white arrow). Red indicates SMA; yellow, rat Y chromosome; blue, nuclei. **M**, Quantitative analysis of cell survival estimation. GFP-positive cells and rat Y chromosome–positive cells were counted, respectively, and corrected by total number of tissue cells to examine the survival cells quantitatively. **N**, Representative anti–integrin β1 staining of the borderzone myocardium. **O**, Quantification of cell–matrix attachment. Cell–matrix attachment was significantly enhanced in the cell-sheet group compared with the other groups (cell sheet, n=4; cell injection, n=4; control, n=4; *P*=0.01, Kruskal–Wallis test).

with injection alone. The robust angiogenic effect of bi-level cell-sheet translated to enhanced myocardial function of the ischemic heart.

Our group has investigated the effects of EPCs as a neovasculogenic therapy for ICM using EPC therapy alone,[14] with seeded EPCs,[13] and with a tissue-engineered matrix.[2] Based on these findings, we began to explore the effects of ex vivo expanded EPCs. Systemic and direct myocardial injection of EPCs, however, is fraught with complications, such as cell dispersion and high percentages of cell loss. In this study, we used cell-sheet technology, which allows efficient delivery of cells onto the ischemic area of myocardium with minimal myocardial injury and cell dispersion, preserves cell–cell and cell–ECM architectural structure, and might, therefore, be more applicable to human translation.[15]

Given our previous work and experience with cell-sheet technology, one possible mechanism is likely to include cytokine release and hematopoietic stem cell recruitment.[7–9] Previous studies have shown that EPCs acted as the natural supplier of SDF1α,[16] VEGF,[17] HGF,[18] and TGFβ.[19] Their roles and signaling pathways have been intensively investigated; SDF1α is related to cell migration, proliferation, and migration[2,13,16]; VEGF is critical to stimulate endothelial cell proliferation and migration to initiate neovascularization[19]; HGF is beneficial to an impaired heart and is associated with an antifibrotic effect.[7,20] Together with our findings, it is reasonable to conclude that coculturing EPCs with SMCs enhanced the secretion of cytokines, such as SDF1α, VEGF, HGF, and TGFβ, compared with either EPCs or SMCs, thus leading to the enhanced proliferation of cardiomyocytes and stimulation of angiogenesis. To understand the detailed mechanism by which coculturing enhances cytokine secretion, we performed additional investigations from a new perspective. We found that FLK1 and VEGFR2 were upregulated by additional VEGF, which were even more enhanced by numerous cytokines containing cell-culturing medium, suggesting that multiple growth factors evoked the upregulation of FLK1 and VEGFR2 expressions over the single factor (ie, VEGF), thereby possibly amplifying VEGF release. The understanding of our results may be translated into the emerging concept that SMCs support the biological aspects of EPCs via the endothelial–pericyte cytokine cross-communication.

The mechanism of restoration of damaged myocardium by EPC transplantation is complex.[2,3,13] Although cytokine release and hematopoietic stem cell recruitment have been proposed as possible mechanisms of regeneration, other important mechanisms are likely to be involved. The creation of mature, stable, and functional vessels is essential. It has been reported

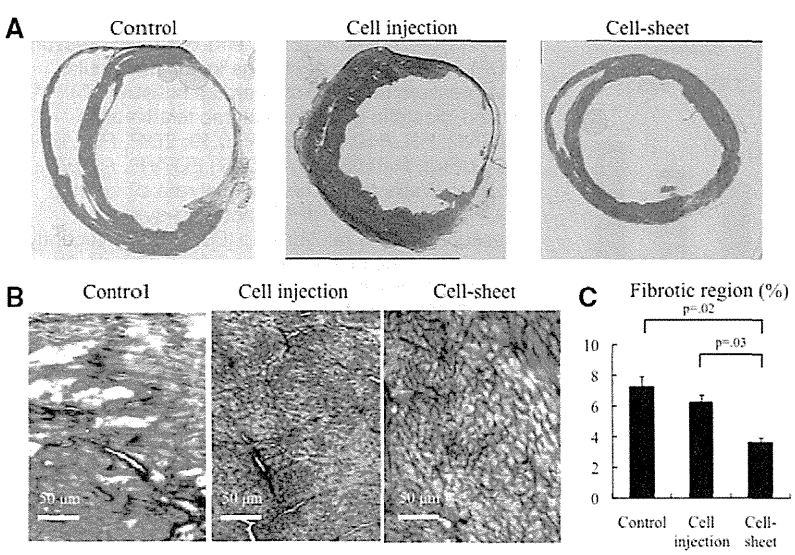

Figure 5. A, Representative macroscopic views of the heart (hematoxylin-eosin staining). The myocardial structure was superiorly maintained after cell-sheet transplantation compared with cell injection and control. **B**, Representative Masson trichrome staining at the borderzone myocardium. **C**, Quantification of fibrotic region. Fibrosis at the borderzone area was significantly suppressed in the cell-sheet group compared with the other groups (cell sheet, n=4; cell injection, n=3; control, n=4; *P*=0.02, Kruskal–Wallis test).

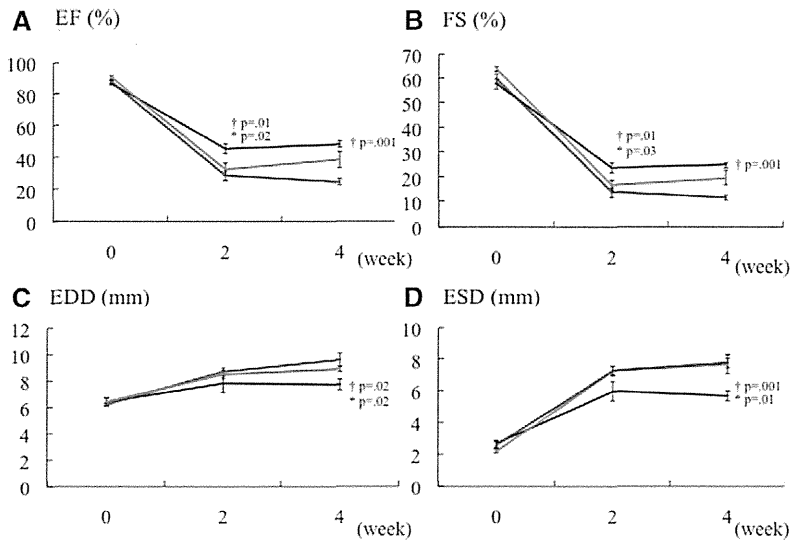

Figure 6. Serial changes in (**A**) ejection fraction (EF), (**B**) fractional shortening (FS), (**C**) end-diastolic diameter (EDD), and (**D**) end-systolic diameter (ESD) assessed by echocardiography (cell sheet, n=7, black line; cell injection, n=8, red line; control, n=9, blue line). Examinations were performed before (0) and at 2 and 4 weeks of follow-up after the operation. EF and FS were significantly higher at 2 and 4 weeks in the cell-sheet group compared with either cell injection or control (EF at 2 weeks, *P*=0.01; EF at 4 weeks, *P*=0.003; FS at 2 weeks, *P*=0.01; FS at 4 weeks, *P*=0.003; Kruskal–Wallis test). EDD and ESD were lowest at 4 weeks in the cell-sheet group (EDD, *P*=0.02; ESD, *P*=0.003; Kruskal–Wallis test). **P*<0.05 vs cell injection; †*P*<0.05 vs control, post hoc pairwise Wilcoxon–Mann–Whitney *U* test.

that capillary formation occurs via two basic vessel-constructing processes: angiogenesis (ie, the formation of new capillaries via sprouting or intussusception from preexisting vessels) and vasculogenesis (ie, de novo formation of vasculature as occurs in the developing embryo).[21] It has also been reported that angiogenesis requires a dynamic temporally and spatially regulated interaction among endothelial cells, pericytes, and angiogenic factors.[22] Given the natural relationship between endothelium and intima within mature vessels, we added SMCs, which are essentially vascular pericytes, to enhance the angiogenic performance of EPCs. Thus, it was hypothesized that coculturing EPCs with SMCs would promote a robust angiogenic response and induce formation of mature blood vessels. Our present study shows that in addition to the

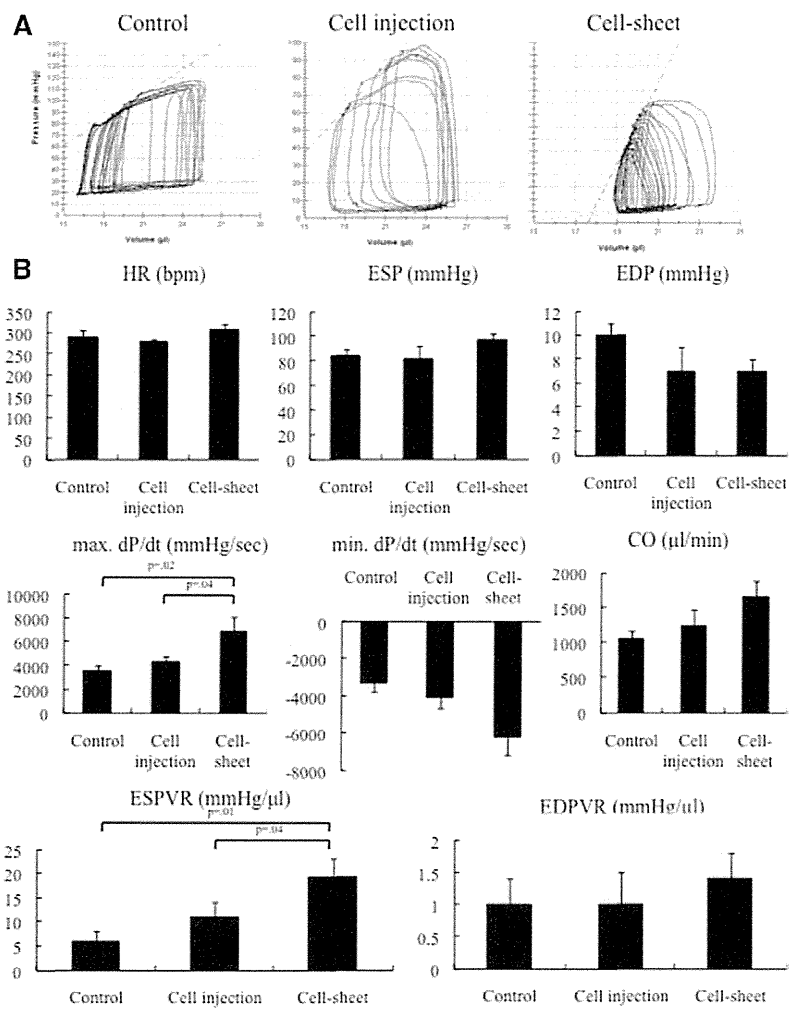

Figure 7. Hemodynamic measurements determined using cardiac catheterization after cocultured bi-level cell-sheet transplantation (cell-sheet, n=6), cocultured cell injection (cell injection, n=6), and control (control, n=8). Examinations were performed at 4 weeks of follow-up after the operation. **A**, Representative pressure–volume loops during inferior vena cava occlusion from cell-sheet, cell injection, and control groups. **B**, There was no significant difference in heart rate (HR), end-systolic pressure (ESP), end-diastolic pressure (EDP), mimimal rate of change in left ventricular (LV) pressure (min. d*P*/d*t*), cardiac output (CO), or end-diastolic pressure–volume relationship (EDPVR; HR, *P*=0.35; ESP, *P*=0.19; EDP, *P*=0.14; min. d*P*/d*t*, *P*=0.05; CO, *P*=0.07; EDPVR, *P*=0.70; Kruskal–Wallis test). The maximal rate of change in LV pressure (max. d*P*/d*t*) and end-systolic pressure–volume relationship (ESPVR) significantly improved in the cell-sheet group compared with the other 2 groups (max. d*P*/d*t*, *P*=0.04; ESPVR, *P*=0.03; Kruskal–Wallis test).

increased capillary density and organized capillary network in the engineered myocardial tissues, enhanced GFP-labeled EPCs originating from the transplanted cell sheet seemed to differentiate into an inner vWF- and vascular endothelial-cadherin–positive endothelial layer surrounded by an outer circumferential SMA-positive layer, partially derived from transplanted SMCs. The direct contribution of SMCs was confirmed by fluorescence in situ hybridization analysis of the myocardium, demonstrating new vasculature containing male SMCs in a female heart. Furthermore, the morphology of the vessel formation within myocardial tissues, including the diameter, composition, and stability of vessel walls, suggested that vessel maturation may occur under pathological stimuli. Furthermore, our data showed that coculturing EPCs with SMCs enhanced the secretion of TGFβ, which is thought to promote stabilization in multiple ways: the synthesis and deposition of ECM and contextual regulation of proliferation and differentiation.[17] Therefore, it is likely that the process of vessel maturation is a transition from an actively growing vessel to a quiescent fully functional mature vessel network via endothelial–pericyte interaction.

The mechanism by which the transplanted cocultured bi-level cell sheet attenuated ventricular remodeling and improved cardiac function, as shown in this study, seemed to depend on the cell sheet being placed over the scarred area of the myocardium and led to repair of the anterior wall thickness, reduction of LV wall stress, and the improvement of LV function. Previous studies indicated that the surviving myocardium and transplanted cell sheet attenuate complex cellular and molecular events, including hypertrophy, fibrosis, apoptosis of the myocardium, and the pathological accumulation of ECM.[7,23]

Cell engraftment is another critical aspect of myocardial regeneration. The potential advantages of the cell-sheet technology include the ability to deliver a larger number of transplanted cells that integrate with native tissues without destroying the cell–cell or cell–ECM adhesions in the cell-sheet.[7] Together with our significant findings of increased cell survival, integrin β1 upregulation, and the enhanced secretion of HGF in vitro in the cell-sheet group, it is likely that the cocultured bi-level cell-sheet prolonged cell survival by preventing anoikis mediated by the ECM receptors, in particular via integrin β1, or modulated by growth factor (eg, HGF).[24]

This treatment strategy for acute myocardial infarction is not yet directly applicable to the clinical arena because of the time required to isolate, cultivate, and manipulate cells in vitro However, the finding that this therapy yielded marked cardioprotective effects through angiogenesis should be beneficial for treating other types of cardiac pathologies, such as the chronic phase of myocardial infarction.

A potential limitation of this study is that the optimal number of transplanted cells was unknown in vivo. In addition, further studies are necessary to determine the optimal mixing ratio of transplanted EPCs and SMCs. We believe that this scaffold-free cell-sheet technique seems to be more transplantable to humans.[15] Although the cocultured bi-level cell sheet maintained different cell types in separate layers in vitro, our in vivo findings showed that the transplanted cell sheet could be a mixture of both cell types. This is probably because each cell type possessed different cell affinity, cell–matrix attachment, and migration ability.

In conclusion, we found that coculturing EPCs with SMCs in a bi-level cell-sheet delivery system enhanced the angiogenic effect by facilitating more architecturally mature microvascular formation. We also observed that bi-level cell-sheet technology initiated robust angiogenesis and regulated vessel maturation, thereby reducing fibrosis, attenuating ventricular remodeling, and improving cardiac function in ischemic cardiomyopathic rats. These findings suggest that novel bi-level cell-sheet technology creates an avenue of powerful cardiac repair. This concept may lead to new regeneration therapies in advanced cardiomyopathy.

Acknowledgments

We thank Dr Arudo Hiraoka, Dr Masaki Taira, and Akima Harada for their excellent technical assistances. We also thank Dr Takashi Daimon, Department of Biostatistics, Hyogo College of Medicine, for his statistical assessment.

Sources of Funding

This study was supported by the National Institutes of Health grant 1R01HL089315 (to Dr Woo), the American Heart Association Great Rivers Affiliate Postdoctoral Fellowship cosponsored by the Claude R. Joyner Fund for Young Medical Researchers (No. 12POST12060567; to Dr Shudo), and the Shinya Fund for International Exchange, Japan (Dr Shudo).

Disclosures

None.

References

1. Hiesinger W, Perez-Aguilar JM, Atluri P, Marotta NA, Frederick JR, Fitzpatrick JR 3rd, McCormick RC, Muenzer JR, Yang EC, Levit RD, Yuan LJ, Macarthur JW, Saven JG, Woo YJ. Computational protein design to reengineer stromal cell-derived factor-1α generates an effective and translatable angiogenic polypeptide analog. *Circulation*. 2011;124(11 suppl):S18–S26.
2. Frederick JR, Fitzpatrick JR 3rd, McCormick RC, Harris DA, Kim AY, Muenzer JR, Marotta N, Smith MJ, Cohen JE, Hiesinger W, Atluri P, Woo YJ. Stromal cell-derived factor-1alpha activation of tissue-engineered endothelial progenitor cell matrix enhances ventricular function after myocardial infarction by inducing neovasculogenesis. *Circulation*. 2010;122(11 suppl):S107–S117.
3. Atluri P, Panlilio CM, Liao GP, Hiesinger W, Harris DA, McCormick RC, Cohen JE, Jin T, Feng W, Levit RD, Dong N, Woo YJ. Acute myocardial rescue with endogenous endothelial progenitor cell therapy. *Heart Lung Circ*. 2010;19:644–654.
4. Hagège AA, Marolleau JP, Vilquin JT, Alhéritière A, Peyrard S, Duboc D, Abergel E, Messas E, Mousseaux E, Schwartz K, Desnos M, Menasché P. Skeletal myoblast transplantation in ischemic heart failure: long-term follow-up of the first phase I cohort of patients. *Circulation*. 2006;114(1 suppl):I108–I113.
5. Schächinger V, Erbs S, Elsässer A, Haberbosch W, Hambrecht R, Hölschermann H, Yu J, Corti R, Mathey DG, Hamm CW, Süselbeck T, Assmus B, Tonn T, Dimmeler S, Zeiher AM; REPAIR-AMI Investigators. Intracoronary bone marrow-derived progenitor cells in acute myocardial infarction. *N Engl J Med*. 2006;355:1210–1221.
6. Assmus B, Honold J, Schächinger V, Britten MB, Fischer-Rasokat U, Lehmann R, Teupe C, Pistorius K, Martin H, Abolmaali ND, Tonn T, Dimmeler S, Zeiher AM. Transcoronary transplantation of progenitor cells after myocardial infarction. *N Engl J Med*. 2006;355:1222–1232.
7. Miyagawa S, Roth M, Saito A, Sawa Y, Kostin S. Tissue-engineered cardiac constructs for cardiac repair. *Ann Thorac Surg*. 2011;91:320–329.
8. Imanishi Y, Miyagawa S, Maeda N, Fukushima S, Kitagawa-Sakakida S, Daimon T, Hirata A, Shimizu T, Okano T, Shimomura I, Sawa Y. Induced adipocyte cell-sheet ameliorates cardiac dysfunction in a mouse

myocardial infarction model: a novel drug delivery system for heart failure. *Circulation*. 2011;124(11 suppl):S10–S17.
9. Shudo Y, Miyagawa S, Fukushima S, Saito A, Shimizu T, Okano T, Sawa Y. Novel regenerative therapy using cell-sheet covered with omentum flap delivers a huge number of cells in a porcine myocardial infarction model. *J Thorac Cardiovasc Surg*. 2011;142:1188–1196.
10. Sekine H, Shimizu T, Hobo K, Sekiya S, Yang J, Yamato M, Kurosawa H, Kobayashi E, Okano T. Endothelial cell coculture within tissue-engineered cardiomyocyte sheets enhances neovascularization and improves cardiac function of ischemic hearts. *Circulation*. 2008;118(14 suppl):S145–S152.
11. Kobayashi H, Shimizu T, Yamato M, Tono K, Masuda H, Asahara T, Kasanuki H, Okano T. Fibroblast sheets co-cultured with endothelial progenitor cells improve cardiac function of infarcted hearts. *J Artif Organs*. 2008;11:141–147.
12. Dzau VJ, Braun-Dullaeus RC, Sedding DG. Vascular proliferation and atherosclerosis: new perspectives and therapeutic strategies. *Nat Med*. 2002;8:1249–1256.
13. Atluri P, Liao GP, Panlilio CM, Hsu VM, Leskowitz MJ, Morine KJ, Cohen JE, Berry MF, Suarez EE, Murphy DA, Lee WM, Gardner TJ, Sweeney HL, Woo YJ. Neovasculogenic therapy to augment perfusion and preserve viability in ischemic cardiomyopathy. *Ann Thorac Surg*. 2006;81:1728–1736.
14. Asahara T, Murohara T, Sullivan A, Silver M, van der Zee R, Li T, Witzenbichler B, Schatteman G, Isner JM. Isolation of putative progenitor endothelial cells for angiogenesis. *Science*. 1997;275:964–967.
15. Sawa Y, Miyagawa S, Sakaguchi T, Fujita T, Matsuyama A, Saito A, Shimizu T, Okano T. Tissue engineered myoblast sheets improved cardiac function sufficiently to discontinue LVAS in a patient with DCM: report of a case. *Surg Today*. 2012;42:181–184.
16. Urbich C, Aicher A, Heeschen C, Dernbach E, Hofmann WK, Zeiher AM, Dimmeler S. Soluble factors released by endothelial progenitor cells promote migration of endothelial cells and cardiac resident progenitor cells. *J Mol Cell Cardiol*. 2005;39:733–742.
17. Li M, Nishimura H, Iwakura A, Wecker A, Eaton E, Asahara T, Losordo DW. Endothelial progenitor cells are rapidly recruited to myocardium and mediate protective effect of ischemic preconditioning via "imported" nitric oxide synthase activity. *Circulation*. 2005;111:1114–1120.
18. Rehman J, Li J, Orschell CM, March KL. Peripheral blood "endothelial progenitor cells" are derived from monocyte/macrophages and secrete angiogenic growth factors. *Circulation*. 2003;107:1164–1169.
19. Coussens LM, Werb Z. Inflammation and cancer. *Nature*. 2002;420:860–867.
20. Madonna R, Rokosh G, De Caterina R, Bolli R. Hepatocyte growth factor/Met gene transfer in cardiac stem cells–potential for cardiac repair. *Basic Res Cardiol*. 2010;105:443–452.
21. Risau W. Mechanisms of angiogenesis. *Nature*. 1997;386:671–674.
22. Goumans MJ, Valdimarsdottir G, Itoh S, Rosendahl A, Sideras P, ten Dijke P. Balancing the activation state of the endothelium via two distinct TGF-beta type I receptors. *EMBO J*. 2002;21:1743–1753.
23. Golocheikine A, Tiriveedhi V, Angaswamy N, Benshoff N, Sabarinathan R, Mohanakumar T. Cooperative signaling for angiogenesis and neovascularization by VEGF and HGF following islet transplantation. *Transplantation*. 2010;90:725–731.
24. Zvibel I, Smets F, Soriano H. Anoikis: roadblock to cell transplantation? *Cell Transplant*. 2002;11:621–630.

Evaluation of intramitochondrial ATP levels identifies G0/G1 switch gene 2 as a positive regulator of oxidative phosphorylation

Hidetaka Kioka[a,b,1], Hisakazu Kato[a,1], Makoto Fujikawa[c], Osamu Tsukamoto[a], Toshiharu Suzuki[d,e], Hiromi Imamura[f], Atsushi Nakano[a,g], Shuichiro Higo[a,b], Satoru Yamazaki[h], Takashi Matsuzaki[b], Kazuaki Takafuji[i], Hiroshi Asanuma[j], Masanori Asakura[g], Tetsuo Minamino[b], Yasunori Shintani[a], Masasuke Yoshida[e], Hiroyuki Noji[k], Masafumi Kitakaze[g], Issei Komuro[b,l], Yoshihiro Asano[a,b,2], and Seiji Takashima[a,2]

Departments of [a]Medical Biochemistry and [b]Cardiovascular Medicine and [i]Center for Research Education, Osaka University Graduate School of Medicine, Osaka 565-0871, Japan; [c]Department of Biochemistry, Faculty of Pharmaceutical Science, Tokyo University of Science, Chiba 278-8510, Japan; [d]Chemical Resources Laboratory, Tokyo Institute of Technology, Yokohama 226-8503, Japan; [e]Department of Molecular Bioscience, Kyoto Sangyo University, Kyoto 603-8555, Japan; [f]The Hakubi Center for Advanced Research and Graduate School of Biostudies, Kyoto University, Kyoto 606-8501, Japan; Departments of [g]Clinical Research and Development and [h]Cell Biology, National Cerebral and Cardiovascular Center Research Institute, Osaka 565-8565, Japan; [j]Department of Cardiovascular Science and Technology, Kyoto Prefectural University School of Medicine, Kyoto 602-8566, Japan; and [k]Department of Applied Chemistry, School of Engineering and [l]Department of Cardiovascular Medicine, Graduate School of Medicine, University of Tokyo, Tokyo 113-8656, Japan

Edited by Gottfried Schatz, University of Basel, Reinach, Switzerland, and approved November 19, 2013 (received for review October 7, 2013)

The oxidative phosphorylation (OXPHOS) system generates most of the ATP in respiring cells. ATP-depleting conditions, such as hypoxia, trigger responses that promote ATP production. However, how OXPHOS is regulated during hypoxia has yet to be elucidated. In this study, selective measurement of intramitochondrial ATP levels identified the hypoxia-inducible protein G0/G1 switch gene 2 (G0s2) as a positive regulator of OXPHOS. A mitochondria-targeted, FRET-based ATP biosensor enabled us to assess OXPHOS activity in living cells. Mitochondria-targeted, FRET-based ATP biosensor and ATP production assay in a semi-intact cell system revealed that G0s2 increases mitochondrial ATP production. The expression of G0s2 was rapidly and transiently induced by hypoxic stimuli, and G0s2 interacts with OXPHOS complex V (F_oF_1-ATP synthase). Furthermore, physiological enhancement of G0s2 expression prevented cells from ATP depletion and induced a cellular tolerance for hypoxic stress. These results show that G0s2 positively regulates OXPHOS activity by interacting with F_oF_1-ATP synthase, which causes an increase in ATP production in response to hypoxic stress and protects cells from a critical energy crisis. These findings contribute to the understanding of a unique stress response to energy depletion. Additionally, this study shows the importance of assessing intramitochondrial ATP levels to evaluate OXPHOS activity in living cells.

energy metabolism | live-cell imaging

Maintaining cellular homeostasis and activities requires a stable energy supply. Most eukaryotic cells generate ATP as their energy currency mainly through the mitochondrial oxidative phosphorylation (OXPHOS) system. The OXPHOS system consists of five large protein complex units (i.e., complexes I–V), comprising more than 100 proteins. In this system, oxygen (O_2) is essential as the terminal electron acceptor for complex IV to finally produce the proton-motive force that drives the ATP-generating molecular motor complex V (F_oF_1-ATP synthase).

Hypoxia causes the depletion of intracellular ATP and triggers adaptive cellular responses to help maintain intracellular ATP levels and minimize any deleterious effects of energy depletion. Although the metabolic switch from mitochondrial respiration to anaerobic glycolysis is widely recognized (1–4), several recent reports have shown that hypoxic stimuli unexpectedly increase OXPHOS efficiency as well (5–7). In other words, cells have adaptive mechanisms to maintain intracellular ATP levels by enhancing OXPHOS, particularly in the early phase of hypoxia, in which the O_2 supply is limited but still remains. However, the mechanism by which OXPHOS is regulated during this early hypoxic phase is still not fully understood.

Revealing the mechanism of this fine-tuned regulation of OXPHOS requires accurate and noninvasive measurements of OXPHOS activity. Although researchers have established methods to measure OXPHOS activity, precise measurement, especially in living cells, is still difficult. Measuring the intracellular ATP concentration is one of the most commonly used methods for evaluating OXPHOS activity. However, there are two major problems with this method. First, the intracellular ATP concentration does not always accurately reflect OXPHOS activity, because it can also be affected by glycolytic ATP production, cytosolic ATPases, and ATP buffering enzymes, such as creatine kinase and adenylate kinase (8). Second, because measurements of the ATP concentration by chromatography (9), MS (10), NMR (11), or luciferase assays (12) are based on cell extract analysis, these methods cannot be used to measure the serial ATP concentration changes *in living cells in real time*.

In this study, we overcame these problems by the selective measurement of the intramitochondrial matrix ATP concentration ($[ATP]_{mito}$) in living cells. In the final step of OXPHOS, ATP is produced not in the cytosol but in the mitochondrial matrix. Therefore, we hypothesized that a selectively measuring $[ATP]_{mito}$ is suitable for the highly sensitive evaluation of cellular ATP production by OXPHOS. In fact, real-time evaluation of both $[ATP]_{mito}$ and the cytosolic ATP concentration ($[ATP]_{cyto}$) in living cells revealed that $[ATP]_{mito}$ reflected OXPHOS activity with far more sensitivity than $[ATP]_{cyto}$. Using this fine method, we found that G0/G1 switch gene 2 (G0s2), a hypoxia-induced

Significance

We developed a sensitive method to assess the activity of oxidative phosphorylation in living cells using a FRET-based ATP biosensor. We then revealed that G0/G1 switch gene 2, a protein rapidly induced by hypoxia, increases mitochondrial ATP production by interacting with F_oF_1-ATP synthase and protects cells from a critical energy crisis.

Author contributions: Y.A. and S.T. designed research; H. Kioka, H. Kato, O.T., and A.N. performed research; M.F., T.S., H.I., S.H., S.Y., T. Matsuzaki, K.T., H.A., M.A., T. Minamino, Y.S., M.Y., H.N., M.K., and I.K. contributed new reagents/analytic tools; H. Kioka and H. Kato analyzed data; and Y.A. and S.T. wrote the paper.

The authors declare no conflict of interest.

This article is a PNAS Direct Submission.

[1]H. Kioka and H. Kato contributed equally to this work.

[2]To whom correspondence may be addressed. E-mail: asano@cardiology.med.osaka-u.ac.jp or takasima@cardiology.med.osaka-u.ac.jp.

This article contains supporting information online at www.pnas.org/lookup/suppl/doi:10.1073/pnas.1318547111/-/DCSupplemental.

protein in cardiomyocytes, increases OXPHOS activity. G0s2 interacted with F_oF_1-ATP synthase and increased the ATP production rate. Our results suggest that hypoxia-induced protein G0s2 is a positive regulator of OXPHOS and protects cells by preserving ATP production, even under hypoxic conditions.

Results

Establishment of a Sensitive Method to Assess OXPHOS Activity in Living Cells. To elucidate the mechanism by which OXPHOS is regulated under hypoxia, it is essential to establish a sensitive method for assessing OXPHOS activity in living cells. For this purpose, we used an ATP indicator based on ε-subunit for analytical measurements (ATeam), which is an ATP-sensing FRET-based indicator (13). We introduced this ATP biosensor into cardiomyocytes that possess an abundance of mitochondria and produce the highest levels of ATP among all primary cells (14, 15). The ATeam assay can measure both $[ATP]_{cyto}$ (i.e., the Cyto-ATeam assay) and $[ATP]_{mito}$ when a duplex of the mitochondrial targeting signal of cytochrome *c* oxidase subunit VIII is attached to the indicator (i.e., the Mit-ATeam assay). In this case, the YFP/CFP emission ratio of the ATeam fluorescence represents the ATP concentration in each compartment. Interestingly, the Mit-ATeam assay was a far more sensitive method than the Cyto-ATeam assay in determining OXPHOS activity in living cells. For example, a very low dose of oligomycin A (0.01 μg/mL), a specific OXPHOS complex V (F_oF_1-ATP synthase) inhibitor, greatly reduced the YFP/CFP emission ratio of the Mit-ATeam fluorescence that represents $[ATP]_{mito}$ within 10 min (Fig. 1 *A*, *Upper* and *B* and Movie S1). In contrast, the same dose of oligomycin A resulted in a slight and slow decline of the YFP/CFP emission ratio of Cyto-ATeam fluorescence (Fig. 1 *A*, *Lower* and *B* and Movie S1). The same phenomenon was observed when the cells were exposed to hypoxia, which suppresses the activity of OXPHOS complex IV (cytochrome *c* oxidase). Again, $[ATP]_{mito}$ decreased more markedly than $[ATP]_{cyto}$ during 2.5 h of hypoxia (Fig. 1 *C* and *D* and Movie S2). These results indicate that the Mit-ATeam assay is far more sensitive for measuring the activity of OXPHOS than the Cyto-ATeam assay. In addition, OXPHOS inhibition decreased the YFP/CFP emission ratio of the Mit-ATeam fluorescence of HeLa cells as well as cardiomyocytes (Fig. S1), suggesting the broad applicability of this assay. Therefore, we used Mit-ATeam for the assessment of the OXPHOS activity in living cells.

Hypoxia-Induced Gene G0s2 Affects the Intramitochondrial ATP Concentration. The expression of genes involved in OXPHOS regulation is considered to be up-regulated in the early phase of hypoxia. Thus, to find unique OXPHOS regulators, we focused on the rapidly induced genes in response to hypoxic stimulation. We compared the gene expression profiles of cultured rat cardiomyocytes at three different time points during hypoxic conditions (0, 2, and 12 h) (Fig. S2*A*). The expression of well-known hypoxia-induced genes, such as VEGF-α and hexokinase 2 mRNA (16, 17), was slightly up-regulated at 2 h and further enhanced at 12 h of hypoxia. In contrast, three other genes (*Adamts1*, *Cdkn3*, and *G0s2*) underwent rapid increases in expression at 2 h but declined at 12 h of sustained hypoxia (Fig. S2 *B* and *C*). This rapid and transient time course of expression implies that these three genes may play distinct regulatory roles, especially in the early hypoxic phase, in which oxygen is limited but still available. To examine whether these genes are involved in the regulation of OXPHOS activity, we knocked down these genes by shRNA (see Fig. S7*A*) and examined $[ATP]_{mito}$ using the Mit-ATeam assay. In this experiment, $[ATP]_{mito}$ in cardiomyocytes treated with shRNA for G0s2 clearly declined within 24 h compared with the control cardiomyocytes (Fig. 2*A* and Movie S3). In addition, the time course of ATP decline was in agreement with the time course of G0s2 depletion (Fig. 2*A* and Fig. S3*A*). Importantly, the overexpression of G0s2 restored normal ATP levels (Fig. 2 *B* and *C*), and again, the Cyto-ATeam assay could not detect a significant effect of G0s2 knockdown within this time frame (Fig. S3*B* and Movie S4). These findings imply that mitochondrial ATP production through OXPHOS was inhibited by G0s2 ablation. We confirmed that the mRNA and protein levels of G0s2 both increased after 2–6 h of hypoxia and then declined after 12 h of hypoxia (Fig. 2 *D* and *E*). G0s2 was first reported as a gene with

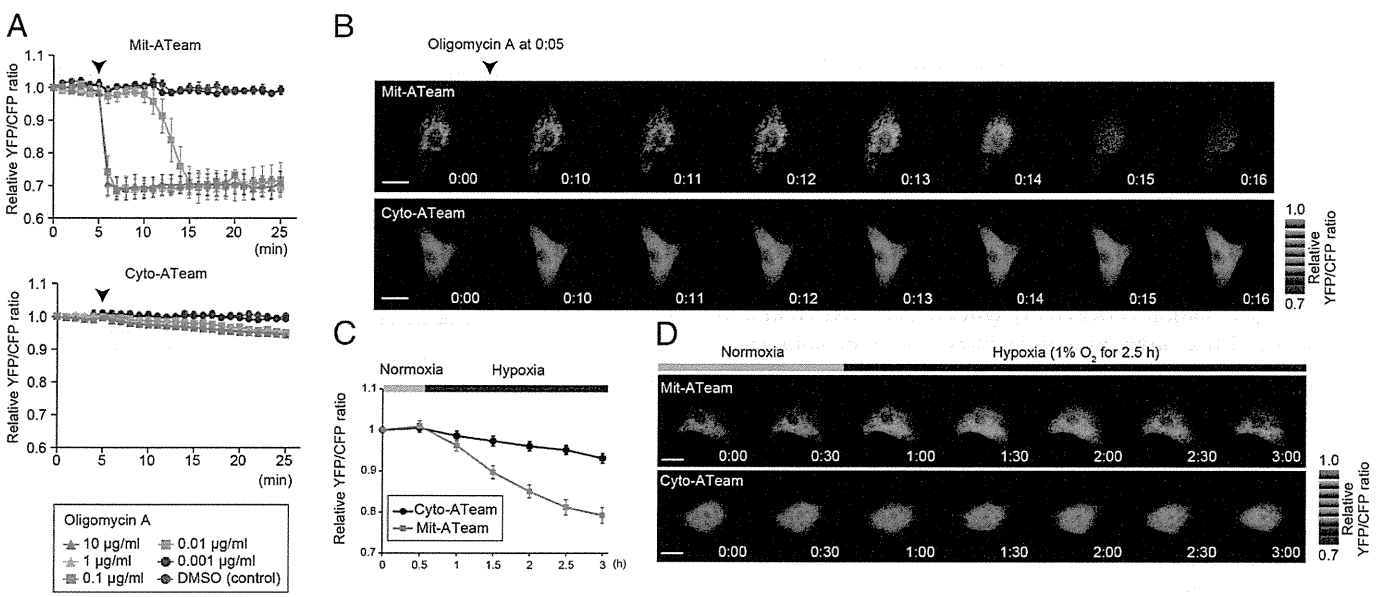

Fig. 1. Establishment of a sensitive method to assess OXPHOS activity in living cells. (*A*) YFP/CFP emission ratio plots of (*Upper*) Mit-ATeam and (*Lower*) Cyto-ATeam fluorescence in cardiomyocytes. Various concentrations (0.001, 0.01, 0.1, 1, and 10 μg/mL) of oligomycin A or DMSO (control) were added at 5 min (arrowhead; $n = 3$). (*B*) Representative sequential YFP/CFP ratiometric pseudocolored images of (*Upper*) Mit-ATeam and (*Lower*) Cyto-ATeam in cardiomyocytes. Oligomycin A (0.01 μg/mL) was added at 5 min. (Scale bars: 20 μm.) (*C*) YFP/CFP emission ratio plots of Mit-ATeam and Cyto-ATeam fluorescence in cardiomyocytes ($n = 10$). (*D*) Representative sequential YFP/CFP ratiometric pseudocolored images of (*Upper*) Mit-ATeam and (*Lower*) Cyto-ATeam in cardiomyocytes. Cells were exposed to 1% hypoxia from the time point 30 min. All of the measurements were normalized to the YFP/CFP emission ratio at 0 min. Data are represented as the means ± SEMs. (Scale bars: 20 μm.)

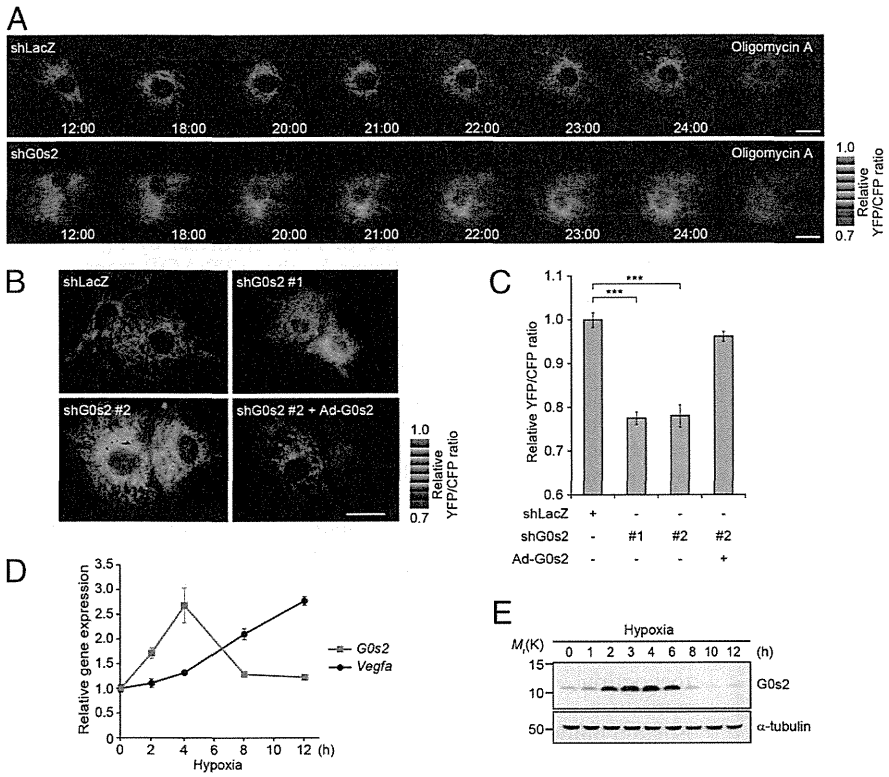

Fig. 2. G0s2, a hypoxia-inducible protein, affects intramitochondrial ATP concentration in cardiomyocytes. (*A*) Sequential YFP/CFP ratiometric pseudocolored images of Mit-ATeam fluorescence in cardiomyocytes expressing (*Upper*) shRNAs for LacZ (shLacZ) or (*Lower*) G0s2 (shG0s2). Oligomycin A (1 μg/mL) was added at the end of the time-lapse imaging to completely inhibit ATP synthesis. The indicated time represents the period after adenovirus infection. (*B*) Representative YFP/CFP ratiometric pseudocolored images of Mit-ATeam fluorescence in cardiomyocytes expressing the indicated adenovirus for 24 h. (Scale bar: *A* and *B*, 20 μm.) (*C*) The bar graph shows the mean YFP/CFP emission ratio of Mit-ATeam fluorescence in cardiomyocytes expressing shLacZ (n = 30), shG0s2 #1 (n = 30), shG0s2 #2 (n = 29), and shG0s2 #2 + G0s2 WT (n = 32) for 24 h. All of the measurements were normalized to the average of the control cells (shLacZ). ***$P < 0.001$. (*D*) Gene expression value plots of *G0s2* (red line) and *VEGF-α* (*Vegfa*; black line) levels in cardiomyocytes under hypoxic conditions (1% O_2). Each value was compared with the level of *Actb* expression (n = 3). Values represent the means ± SEMs. (*E*) Immunoblotting of the G0s2 expression in cardiomyocytes under hypoxic conditions (1% O_2).

expression that was induced during the cell cycle switch from G0 to G1 phase (18). G0s2 is expressed in many tissues and especially abundant in heart, skeletal muscle, liver, kidney, brain, and adipose tissue (19). Although G0s2 may play a role in cell cycle progression (20), the function of G0s2 in the hypoxic response remains unknown.

G0s2 Rescues the Decline of ATP Production During Hypoxia. We next tested whether the overexpression of the G0s2 before hypoxic stress could prevent hypoxia-induced ATP depletion. We prepared cardiomyocytes overexpressing G0s2 and control cardiomyocytes. During sustained hypoxia, $[ATP]_{mito}$ gradually declined in control cardiomyocytes as measured by the Mit-ATeam assay. Notably, the overexpression of G0s2 before the onset of hypoxia reduced this decline in $[ATP]_{mito}$, which allowed the cardiomyocytes to promptly recover to baseline levels of $[ATP]_{mito}$ after reoxygenation (Fig. 3 *A* and *B* and Movie S5). In addition, the prehypoxia overexpression of G0s2 preserved cell viability during sustained hypoxia (Fig. 3*C*). These results suggest that G0s2 can preserve mitochondrial ATP production even under hypoxia and protect cells from the energy crisis under hypoxia.

G0s2 Binds to F_oF_1-ATP Synthase but Not Other OXPHOS Protein Complexes. To reveal the mechanism by which G0s2 affects $[ATP]_{mito}$, we sought to identify the biochemical targets of G0s2. We screened for G0s2 binding proteins by immunoaffinity purification of cell lysates from cardiomyocytes expressing C-terminally Flag-tagged G0s2 (G0s2-Flag). G0s2-Flag is expressed in cardiomyocytes localized to the mitochondria (Fig. S4*A*). MS analysis revealed that multiple F_oF_1-ATP synthase subunits, but no other mitochondrial respiratory chain complex subunits, were coimmunoprecipitated with G0s2-Flag (Fig. S4*B* and Table S1). F_oF_1-ATP synthase is a well-known ATP-producing enzyme composed of a protein complex that contains an extramembranous F_1 and an intramembranous F_o domain linked by a peripheral and a central stalk (21–24). The binding of F_oF_1-ATP synthase to G0s2-Flag was confirmed by immunoblotting with antibodies against several subunits of F_oF_1-ATP synthase (Fig. 4*A*).

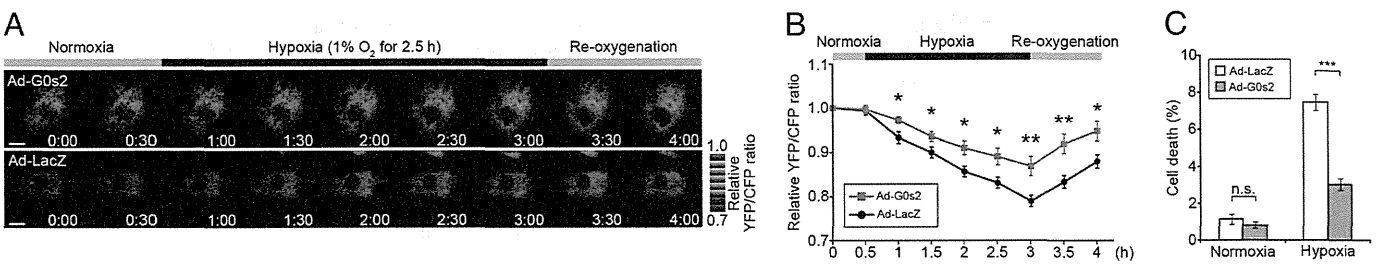

Fig. 3. Overexpression of G0s2 before hypoxia rescues the decline of mitochondrial ATP production during hypoxia. (*A*) Sequential YFP/CFP ratiometric pseudocolored images of Mit-ATeam fluorescence in cardiomyocytes expressing (*Upper*) G0s2 WT or (*Lower*) LacZ during hypoxia and reoxygenation. (Scale bar: 20 μm.) (*B*) YFP/CFP emission ratio plots of Mit-ATeam fluorescence in cardiomyocytes expressing G0s2 WT (n = 20) or LacZ (n = 19) during hypoxia and reoxygenation. All of the measurements were normalized to the ratio at time 0 and compared between cardiomyocytes with G0s2 WT and LacZ at each time point. (*C*) The bar graph shows the cell viability of cardiomyocytes overexpressing G0s2 under hypoxic conditions. Cardiomyocytes expressing either LacZ or G0s2 WT were cultured under normoxic or hypoxic conditions for 18 h (n = 8). The asterisks denote statistical significance comparing G0s2 with LacZ. Data are represented as the means ± SEMs. n.s., not significant. *$P < 0.05$; **$P < 0.01$; ***$P < 0.001$.